

## Response to Reviewers

### Response to Reviewer #1 Matthew Lebsock

I would like to thank Dr. Matthew Lebsock for his insightful and suggestive comments that helped us substantially improve the manuscript. Point-to-point replies to the comments are provided below (reviewer's comments in italic blue font).

#### *General comments:*

*This paper uses Daily gridded Level-3 histograms of MODIS cloud retrievals to derive the small-scale variability in liquid cloud properties, specifically cloud liquid waterpath (lwp) and droplet number concentration(cdnc). This is the first study to address the variance of cdnc from satellite data. The variability is then used to diagnose the expected enhancement of the autoconversion process due to sub-grid scale distribution of cloud fields in global models. The regional variation of the enhancement are shown. Surprisingly the enhancement due to variability in the cdnc is shown to be often larger than that due to lwp.*

*The largest enhancement due to number concentration variability is correlated with number concentration itself. This correlation is largely unexplained and a major result of the paper. There is a limited attempt to attempt to explain the unexpectedly large cdnc enhancement factor based on retrieval uncertainty in broken cloud scenes but the authors should consider physical mechanisms as well. I would suggest that thin detrained veil clouds near precipitating cumulus could be a physical mechanism for seeing this variability in the observations.*

*The science focus of this paper is novel and timely, the methodology is appropriate, and the presentation is generally good. I've included some additional references to add and specific comments below. In terms of additional analysis I would advocate quantifying the correlation between  $E_n$  and other cloud properties on various scales (correlate 1 degree grids (super pixel), correlate spatial patterns) to identify the controlling factors. This will help us better understand what variables might be influencing the high  $E_n$  (i.e. cloud fraction, low optical depth, CDNC, LWP, etc. A Table might work well to present these results.*

Reply: Thanks for the review and helpful comments. Following your suggestions, we made significant revisions to the paper. Major changes include:

- We added more discussions on the correlation between LWP and CDNC and its implications for enhancement factor.
- We also provide some possible physical explanation on the large  $E_N$ . Please see details below.
- Figure 5, 7, 10, 11 are updated.

*Specific comments:*

*Lines 123-128: add Ahlgrim et al., 2016 (<https://doi.org/10.1002/qj.2783>). They also use DOE data and create a parameterization of  $E$  based on cloud fraction.*

Reply: Thanks. The paper is added to the citation list.

*Line 135: Add citation to Takahashi et al., 2017 (<https://doi.org/10.1002/2016JD026404>). They have shown that more advance parameterization, specifically a version of the Multi-scale Modeling Framework model is able to produce reasonable distributions of regional distributions of the cloud water heterogeneity when compared against the satellite observations (their figure 2).*

Reply: Thanks. The paper is added to the citation list.

*Line 137: Somewhere in here you should point out that the estimate of variance depends on the spatial resolution of the observations. With satellite observations (even MODIS) we are using relatively coarse observations and therefore we cannot resolve variance on the smallest scales. So satellite observations will necessarily underestimate variance because of this effect, however, they should provide an accurate assessment of regional distributions of the microphysical process enhancement factors.*

Reply: Good point. Some discussions on the limitations of satellite observations are added after the Lebsock (2013) study.

*Line 146: I wouldn't say that the 'empty cloud' problem is a well defined term. I can guess what this means but I would state explicitly a diagnosis of the problem. Probably there is too much rain and clouds with very low or zero liquid water path at the end of the time step?*

Reply: You are right. "empty clouds" have near-zero cloud water which is caused by excessive rain (Song et al. 2018). This sentence is revised.

*Line 246: I think that  $E_q$  should be  $E_N$  here and cloud water should be CDNC.*

Reply: Thanks for catching this. It is revised.

*Figure 1B/Line 262/Line263, and elsewhere: What is plotted here is not the rain rate. It is rate of conversion cloud water to precipitation water (or the autoconversion process rate). Rain rate is the integral of over the precipitation drop size distribution multiplied by the density-dependent fall velocity for each drop radius. This should be corrected throughout the manuscript.*

Reply: Thanks for pointing this out. We should be more careful. In the revised manuscript, we use "autoconversion rate", instead of "rain rate" throughout the paper.

*Line 318: You should point out that calculating the  $\nu$  parameter in this way can be very sensitive to outliers as the sample size gets small (i.e. low cloud fraction) and there are other methods to calculate  $\nu$  from the data (e.g. Oreopoulos and Cahalan, 2005) that will give different answers.*

Reply: Thanks for pointing this out. Indeed, the method we used in this study is the method of moment (MOM). The inverse relative variance can also be estimated using the maximum likelihood estimate (MLE). We pointed this out in the revised manuscript.

The MODIS level 3 product reports the logarithm mean of cloud optical thickness which enables us to use the MLE method to estimate the  $\nu_{MLE}$  from Eq. 6 of Oreopoulos and Cahalan (2005). The results are shown below compared with the value from the MOM  $\nu_{MOM}$ . Apparently,  $\nu_{MLE}$  tends to be larger than  $\nu_{MOM}$  especially over regions with low water cloud fraction, although the spatial pattern is similar. This is probably because, as you pointed out, the MOM is more prone to the impact of extreme values when cloud fraction is small. Nevertheless, the difference does not change any conclusions.

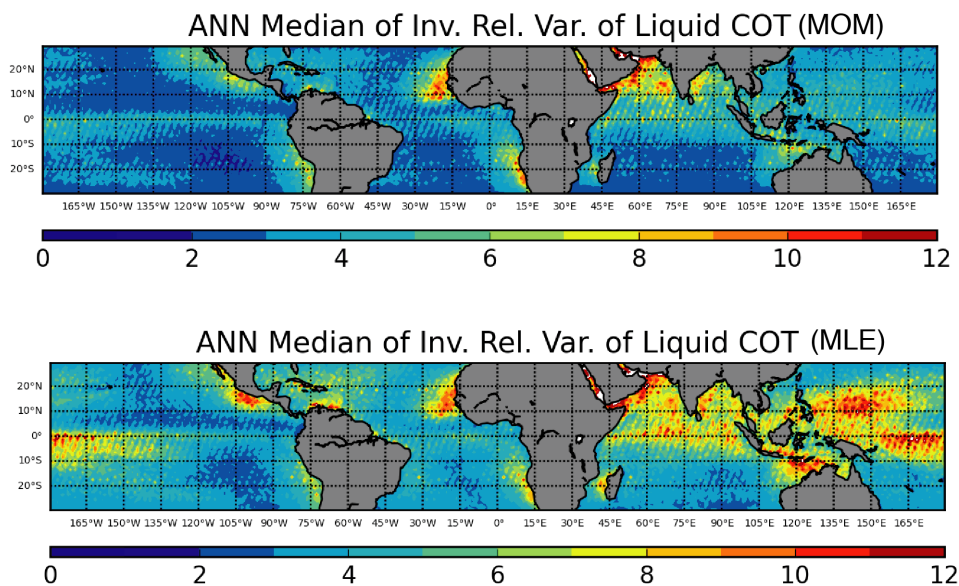


*Figure 5: The caption says these are means, as does panel b. But the other panels say median as does the paper text. Which is it? Median I think. . .*

Reply: It's a typo and should be "Median". Corrected.

*Line 327: Lebsock et al., 2011 (<https://doi.org/10.1175/2010JAMC2494.1>) also argue this about 3.7 micron re.*

Reply: Thanks. This paper is cited in the revised version. Of course, the choice of coefficient for LWP computation does not matter in this study because it is a common

factor in both numerator and denominator in the calculation of  $\nu$ .

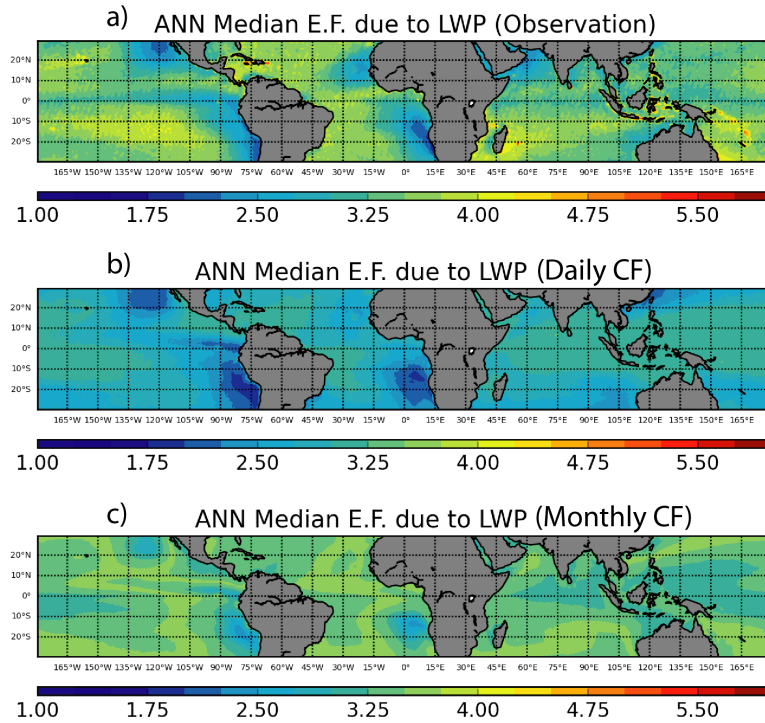
*Figure 8: you should describe in the caption the difference in the fitting so the reader doesn't have to go to the text and equations.*

Reply: Good suggestion. We added the information.

*Figure 8: I do think it is useful to show that the parameterization of  $\nu$  based on cloud fraction does not work because of the non-linearity in the process. However, can you explain why even the parameterization of the enhancement factor directly on cloud fraction under-predicts the direct calculation? That relationship show in 7b is fairly normally distributed so I can't understand why the parameterization would not get the median about right.*

Reply: This is a very good question. To answer it, first let us explain how  $E_q$  in Figure 6 and Fig. 8 are obtained. The parameterization scheme in Eq. (27) and Fig. 7 are developed based on the relation between monthly-mean observation-based  $E_q$  and monthly-mean  $f_{liq}$  in the tropics (i.e., 10 years x 12months x 360 longitude x 60 latitude x fraction of ocean). The sample size would be too large if daily products were used. After we obtained the parameterization scheme (i.e., Eq. 27), we then used it to compute the daily  $E_q$  based on daily  $CF_{liq}$ . The daily  $E_q$  values are then temporally aggregated, weighted by daily  $f_{liq}$ , to first obtain monthly and then annual  $E_q$  in Fig. 8b in the same way as we obtain observed  $E_q$  in Fig. 6. Going back to your question, we think the underestimation of parameterized  $E_q$  (Figure 8b compared to Figure 6a) is due to the fact that the parameterization is developed based on monthly data but applied to daily  $f_{liq}$ . To test this, we applied the parameterization scheme to monthly  $f_{liq}$ . The results are significantly better. See below.





The lesson learned is that the simple parameterization scheme developed based on monthly  $f_{liq}$  cannot capture the day-to-day variation of  $E_q$ , which is not surprising. In our view, the parameterization scheme is only better than assuming a constant  $E_q$  in the sense that it can capture the cloud regime dependence. However, it would be unrealistic to hope that it can simulate the dramatic instantaneous variation. For that, we would have to rely on advanced scheme like CLUBB or MMF.

*Eqs. 26/27 and related discussion: I don't like this parameterization of  $\nu$  based on cloud fraction because it isn't well justified physically. Ideally both the cloud fraction and  $\nu$  could be calculated from either prognostic or diagnostic distribution of the subgrid co-variability of total water and temperature. CLUBB in fact can do this so there should be no need to for such an ad-hoc representation. It is true that such relationships have been advocated in the past but they strike me as very unphysical. I wouldn't advocate this in the context of CLUBB, which is heavily referenced here.*

Reply: We agree with your point about the parameterization of  $\nu$ . The highly non-linear relation between  $\nu$  and the enhancement factor makes the parameterization not so useful. It is shown here simply because some previous studies, e.g. Boulte et al. (2014), Xie and Zhang (2015), had tried to parameterize the  $\nu$  directly. The unsatisfying results motivated us to parameterize the enhancement factor directly.

On the other hand, we think the direct parameterization of enhancement factor is meaningful. It provides with a simple way for those GCMs without advanced sub-grid parameterization scheme to account for the impacts of cloud inhomogeneity on

precipitation simulation. We agree that CLUBB presumably would do a better job than simple parameterization. Nevertheless, the results from this study, including the parameterization of enhancement factor, provide observational basis for evaluating the results from CLUBB.

*Line 603: One physical interpretation of the MODIS retrievals of high effective radii in these broken cloud scenes is that they could be ‘optically thin veil’ clouds as described by O et al. (<https://doi.org/10.1029/2018GL077084>) to be extensive detrained anvil cloud from shallow cumulus with low liquid water content and very low CDNC -> thus potentially large radius. Indeed they are often seen by cloud radar (Wood et al., 2018). Now if this is the case in reality these clouds might contribute quite a bit to the variance in CDNC but shouldn’t lead to any substantial increase in the autoconversion because the low CDNC pixels should also have very low liquid water path -> so the correlation should matter. In fact you show this exact correlation later on.*

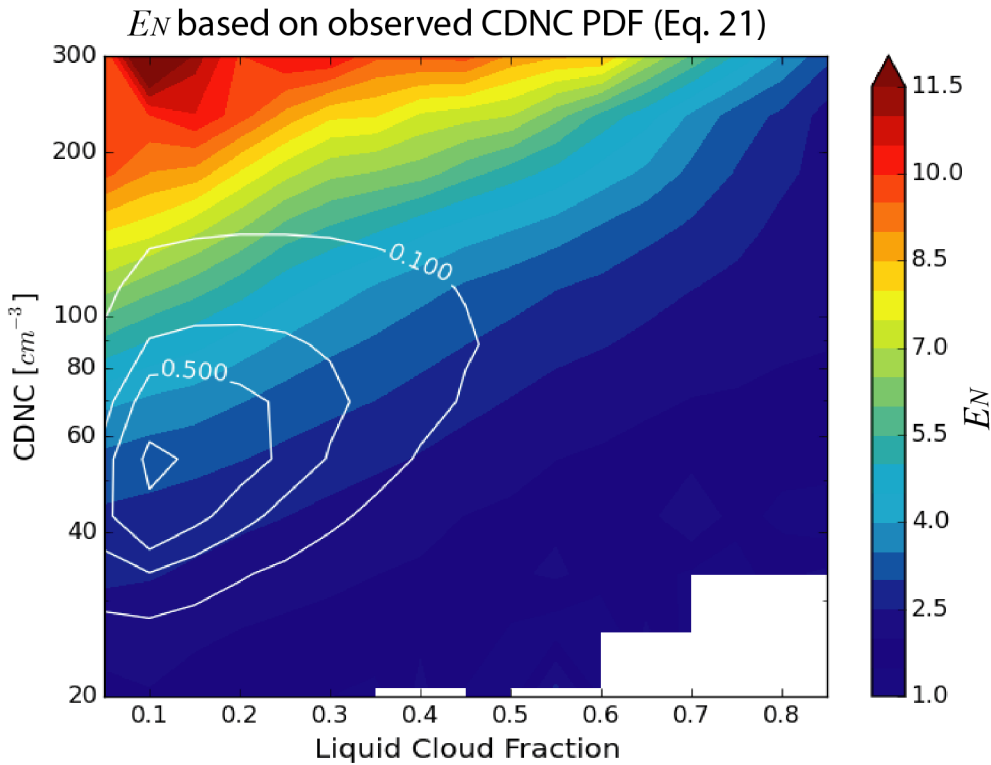
Reply: This is a very insightful comment and thanks for the references (we are aware of Wood et al. 2018 but not O et al.). Following your suggestions, we have de-emphasized the influence of retrieval error and focused more on the potential physical processes that lead to the large subgrid CDNC variance. These papers are now in Section 4 when discuss the new Figure 5 e about the correlation between LWP and CDNC and the its implications.

*Line 603: I think it is important to explore and show some correlations between the  $E_N$  and various other parameters, such as CDNC, cloud fraction, number of pixels with cloud optical depth  $< 4$ . Clearly if some factor is influencing  $E_N$  (Like cloud fraction) you would expect to see some correlation between the variables. You could show either the regional correlations, or do this for individual 1 degree grids. It seems quite clear that there is not a good correlation between liquid cloud fraction and  $E_N$  which doesn’t support the idea that cloud-fraction related retrieval artifacts have much to do with these results. If on the other hand the  $E_N$  mostly correlates with large CDNC, which I suspect it does, then there is a mystery yet to be explained.*

Reply: Thanks for the great suggestions! We made several significant changes to the paper accordingly. We replaced original Figure 10 (which focuses on the retrieval artifacts) with an analysis of the dependence of  $E_N$  on liquid cloud fraction and CDNC. See below. As you suspected,  $E_N$  shows a stronger dependence on CDNC than cloud fraction, which seems to suggest that the dependence is largely due to some underlying physical mechanisms rather than retrieval artifacts. The largest  $E_N$  is usually found where CDNC is large and cloud fraction is small and it decreases with decreasing CDNC and to a less extent also with increasing cloud fraction. The strong dependence of  $E_N$  on CDNC might be explained by the following mechanism in which aerosol plays an important role: when aerosol loading is small, even weak updraft can activate most CCN. As a result, the subgrid turbulence and variance of thermodynamical conditions are not importance leading to small  $E_N$ . In contrast, when aerosol loading is large, subgrid variations of updraft and thermodynamical conditions could lead to significant subgrid variations of CDNC, leading to large  $E_N$ .

In addition to the analysis  $E_N$ , we also added some more in-depth explanation of the importance of LWP and CDNC correlation on enhancement factor simulation at the end of Section 2.2. First, a formula for *combined* enhancement based on the bi-variate lognormal distribution is presented (Eq. 22). Second, we pointed out that the current GCMS, even those with advanced sub-grid parameterization such as CLUBB, only consider the enhancement factor due to LWP  $E_q$ , the effect of  $E_N$  and the correlation term  $E_{COV}$  are ignored. Moreover, an equation is added (Eq. 25) to explain under what circumstances would  $E_q$  underestimate or overestimate the combined effect  $E_q \cdot E_N \cdot E_{COV}$ . In addition, Figure 5 e is added to show the subgrid correlation coefficient of LWP and CDNC and in Figure 11 we discussed the importance of considering  $E_{COV}$  in computing the combined enhancement factor.

We feel that these revisions, based on your suggestions, had made the paper more insightful and more revealing.



*Dependence of  $E_N$  on  $f_{liq}$  and  $N_d$ . The color map corresponds to the mean value of  $E_N$  for a given  $N_d$  and  $f_{liq}$  bin. The white contour lines correspond to the relative sampling frequency of  $N_d$  and  $f_{liq}$  bins (i.e., the most frequently observed combination is  $N_d \sim 50 \text{ cm}^{-3}$  and  $f_{liq} \sim 0.1$ ).*

*Line 646: Again, I think that there may be a physical explanation for this correlation. Specifically that there are a lot of these low water, low  $N$  veil clouds around shallow convection.*

Reply: See our reply above.

*Line 665: I would argue significantly better.*

Reply: agree and revised.

*Line 683: Another example of parameterization that includes subgrid information is the EDMF approach (e.g. Sušelj et al., 2013, <https://doi.org/10.1175/JAS-D-12-0106.1>), variants of which are used in a number of models.*

Reply: we added the EDMF as another example of “advanced subgrid cloud parameterization scheme”. Thanks for pointing it out.

*Technical comments:*

*Line 41 The phrasing ‘clear cloud’ might be confusing. Consider ‘obvious’ or ‘demonstrable’ instead of clear.*

*Line 94: superfluous ‘on’*

*Line 369: the 2~4 notation seems odd to me. I would use ~2-4 COT and ~10-12  $\mu\text{m}$ .*

*Line 402: ‘dominate’ -> ‘dominant’*

*Line 458: missing ‘of’*

*Line 480: grammar, missing word after more. Line*

*493: ‘product’ -> ‘production’*

*Line 496: second 6b should be 6a. Line 497: ‘tend’ -> ‘tends’*

*Line 508: ‘facts’ -> ‘fact’*

*Eqs. 26/27: parenthesis don’t match.*

Reply: Thanks a lot for catching these typos and mistakes. They are all corrected.

I would like to thank the reviewer for the comments and suggestions. Point-to-point replies to the comments are provided below (reviewer's comments in italic blue font).

*Authors derived the subgrid variations of liquid-phase cloud properties over the tropical ocean and investigated the autoconversion enhancement factors using MODIS product. This paper is well written, and of relevance to a broad audience. It is worthy of publication subject to the following issue.*

*(1) Authors assumed that subgrid variation of LWC could be inferred from the spatial variability of LWP. LWP is the vertical integrated LWC over cloud depth, so its subgrid variations include cloud depth variations. But LWC's variations does not. Please justify this assumption.*

Reply: Indeed, MODIS retrievals only provide the LWP instead of the vertically resolved LWC retrieval. This is an important limitation of this study which we pointed out clearly in Section 3.

However, as we also pointed out, other techniques face more or less similar challenge. "We note here that it is the LWC  $q_c$ , instead of the LWP, that is used in the KK2000 scheme. So, the spatial variability of LWC is what is most relevant. However, the remote sensing of cloud water vertical profile from satellite sensor for liquid-phase clouds is extremely challenging even with active sensors. It is why most previous studies using the satellite observations analyzed the spatial variation of LWP, rather than LWC. In fact, even Lebsock et al. (2013), who used the level-2 CloudSat observations, had to use the vertical averaged LWC in their analysis. Airborne in situ measurement faces similar challenge. For example, Boutle et al. (2014) use the LWC observation along "horizontal flight tracks" to study the spatial variability of cloud water, which only samples the LWC at certain levels of MBL clouds. Ground-based observations are much better than satellite and airborne observation in this regard. Recently, Xie and Zhang (2015) analyzed the cloud water profiles retrieved using ground-based radars from the three ARM sites and found no obvious in-cloud vertical dependence of the spatial variability of LWC."

*Typos: (1) Lines 359 ": : :any type of data quality-based data ", Should be ": : :any type of quality-based data".*

*(2) Lines 396 ": : :On the hand ", Should be ": : :On the other hand".*

*(3) Lines 466-467 "...Figure 6 b derived directly from the observation", Should be ": : :Figure 6 a derived directly from the observation."*

Reply: thanks for catching these typos. They are all corrected

I would like to thank the reviewer for the insightful and suggestive comments that helped us substantially improve the manuscript. Point-to-point replies to the comments are provided below (reviewer's comments in italic blue font).

*This paper discusses the GCM sub-grid scale variability of cloud water content and droplet number observed by MODIS, and the consequences this variability has for autoconversion parametrization in GCMs. This has become a popular topic in recent years with many papers discussing the cloud water content variability, although the attempts to discuss droplet number variability are particularly novel and welcome in this study. The paper is well written and interesting. I have compiled a list of relatively minor comments or suggestions that the authors may wish to consider.*

*General comment –*

*the paper is very long, I'd encourage the authors to look for opportunities to be more concise in their descriptions and refrain from repetition of points.*

Reply: The theoretical background part is longer than we hoped but necessary so the readers to understand the studies that followed. The length of the revised version is reduced by one page. It is not trivial considering that we extend the scope of the research significantly.

*L57 - the reference here should be Boutle et al. (2014, QJ) not Boutle & Abel (2012)*

Reply: we updated the references.

*L60-62 - would be good to clarify a couple of things in these lines. Firstly, I think it would be better to refer to autoconversion and accretion "parametrizations" rather than "processes" - we shouldn't confuse the way we parametrize these things with physical reality, as there is not much overlap! Secondly, you should also clarify that you are ignoring variability in rain water content ( $q_r$ ) or  $N_c$ , as the nonlinearity of these (and correlations with  $q_c$ ) could strongly influence the result.*

Reply: Agree, the KK2000 is simply a parameterization based on the least-square fitting to the LES results. We change the wording from "process" to "parameterization" throughout the text whenever appropriate.

We pointed out at the beginning of section 2.2 that we will only focus on the simulation of autoconversion while other processes such as accretion have been investigated in previous studies.



*L92-95, 99-106 - this reads a little harshly on Boutle et al. (2014), who also used CloudSat data in their analysis to give a global perspective (and discussed the increase in variability from Sc to Cu and importance of co-variability on accretion). It might be worth mentioning the study of Hill et al. (2015, QJ) here as well, who extended this work to explicitly build in the regime dependence to the parametrizations. Also there is a typo on L104/5, which should say "cloud water variance is larger over the Cu region than over the Sc region".*

Reply: Agree, we revised the discussion, added the Hill et al. (2015) and also corrected the typo.

*L117-118 - again, might be good to clarify here - Boutle et al. (2014) and Lebsock et al. (2013) discuss the variation in rain water (which is distinct from cloud water). But you are correct that I'm also unaware of any studies looking at CDNC variability.*

Reply: Following your suggestion, we pointed out again that Boutle et al. (2014) and Lebsock et al. (2013) have investigated the variation of subgrid cloud water as well as rain water.

*L194 - would be good to clarify here - it's not the LES that was important in KK2000, but the fact that they used a bin-resolved microphysics scheme, which accurately represented the physical processes of collision-coalescence, to derive the simple parametrizations*

Reply: Agree. In the revised version, we pointed out after the introduction of KK2000 parameterization scheme that the KK2000 is “derived through a least-square fitting of the autoconversion rate results from a large-eddy simulation with bin microphysics that can simulate the process-level physics.”

*Figure 1d - I cannot see this referred to at all in the text, yet it shows something interesting/puzzling to me, namely a significantly different CDF of rain rate for the gamma and lognormal distributions of CDNC - can you explain why this is?*

Reply: As shown in Figure 1, provided the same mean value and same inverse relative variance  $\nu$ , the lognormal distribution  $P_L(x)$  is generally larger than the Gamma distribution  $P_G(x)$ . The difference is clearly visible when  $x > 2.0$  in Figure 1 b. This differences in PDF gives rise to the difference in the CDF of autoconversion rate.

*L256-260 - I'd always thought part of the argument for ignoring Nc is that its value is typically linked to the underlying aerosol distribution, which varies on much larger spatial scales than qc, therefore the amount of Nc variability that would be 'sub-grid' is*

*expected to be small/negligible.*

Reply: Aerosol loading is only on part of the story. CDNC is not only determined by aerosol loading but also critically by the subgrid turbulence (i.e., updraft). Many previous studies have pointed out the importance of subgrid variations of updrafts in simulating cloud microphysics in GCM (e.g., (Morales and Nenes, 2010)). However, most GCMs lack the capability of simulating the subgrid variations of updrafts until very recently the advanced parameterization schemes, such as CLUBB and MMF, became available.

*L274 - please define CER as this has not been previously defined*

Reply: It is clarified.

*L278 - brackets should be around the years only of Platnick et al. (2013,2017)*

Reply: Corrected.

*L344 - I'd say the current generation of GCMs are those being used for CMIP6, so perhaps update this and the reference (although 1x1degree still doesn't seem unreasonable for what many models are running)*

Reply: Updated and added the new reference (Eyring et al., 2016)

*L372 - should say "dominant" cloud types*

Reply: Changed.

*L450 - I think there is something missing from this sentence - "this approach is more although it may be..."*

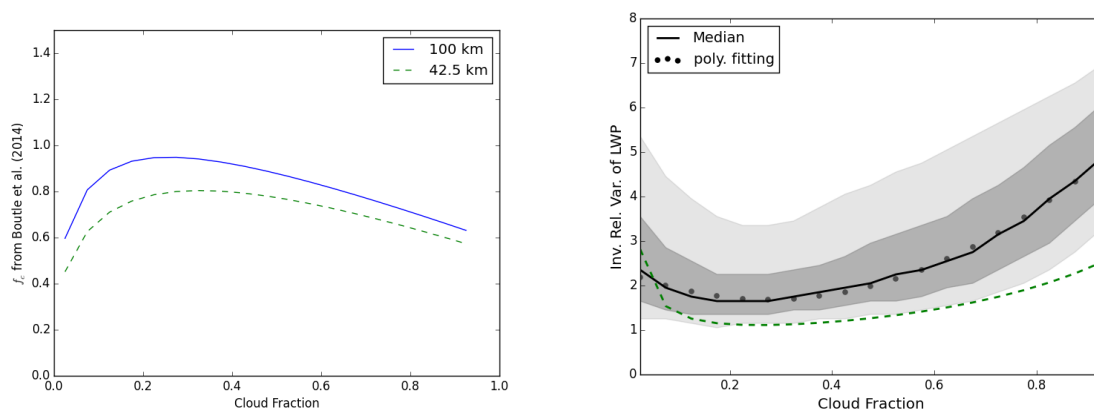
Reply: It should be more "efficient". Corrected.

*Figure 6d - does not appear to be referred to in the text. It should either be discussed why it is relevant, or not shown.*

Reply: It is removed. Thanks for catching this.

*L487-501 - given there is already a parametrization of  $v(f_{liq})$  in existence, namely that of Boutle et al. (2014), it would be interesting and very easy to see how well their parametrization compares to the independent MODIS dataset generated in this study. It's probably too much work to investigate the Hill et al (2015) parametrization as that would require a way of determining from MODIS whether cloud is convective or not, but that would also be interesting.*

Reply: We first replicate the Figure 4 in Boutle et al. (2014) to confirm our code works consistently with the original result.



Then, we compared the parameterization scheme from *Boutle et al. (2014)* for grid size  $\sim 100\text{km}$  to our Figure 7a (the green dashed line). Apparently, there are some differences between the two especially for large cloud fraction, probably because the two studies are based on different data. Since the difference between the two studies are out of the scope of this paper. These figures are not shown in the paper.

*L506-516 - it would also be worth noting that these fits are only applicable to a single model resolution, and so not as useful as existing parametrizations with inbuilt scale adaptiveness.*

Reply: Agree and we already mentioned that this parameterization is only valid for  $1\times 1$  degree model resolution when we list the important limitation of this study.

*L559 - there is reference to supplementary materials, yet I cannot find any?*

Reply: We originally planned to add the seasonal plots (e.g., DJF and JJA) in the supplementary materials, but we found that seasonal plots do not really add any additional insights. So, we simply removed them. Sorry for the confusion.

Boutle, I. A., Abel, S. J., Hill, P. G. and Morcrette, C. J.: Spatial variability of liquid cloud and rain: observations and microphysical effects, *Quarterly Journal of the Royal Meteorological Society*, 140(679), 583–594, doi:10.1002/qj.2140, 2014.

**Reference:**

Boutle, I. A., Abel, S. J., Hill, P. G. and Morcrette, C. J.: Spatial variability of liquid cloud and rain: observations and microphysical effects, *Quarterly Journal of the Royal Meteorological Society*, 140(679), 583–594, doi:10.1002/qj.2140, 2014.

Eyring, V., Bony, S., Meehl, G. A., Senior, C. A., Stevens, B., Stouffer, R. J. and Taylor, K. E.: Overview of the Coupled Model Intercomparison Project Phase 6 (CMIP6) experimental design and organization, *Geosci. Model Dev.*, 9(5), 1937–1958, doi:10.5194/gmd-9-1937-2016, 2016.

Morales, R. and Nenes, A.: Characteristic updrafts for computing distribution-averaged cloud droplet number and stratocumulus cloud properties, *J. Geophys. Res.*, 115(D18), 1227, 2010.

**Style Definition:** MTEquationSection: Hidden

**Formatted:** Font: +Body (Calibri)

**Formatted:** Font: +Body (Calibri)

- Deleted:** System

**Formatted:** Font: +Body (Calibri)

**Formatted:** Font: +Body (Calibri)

**Formatted:** Font: +Body (Calibri)

**Deleted:** For publication in

**Formatted:** Font: +Body (Calibri)

31

32 **Abstract:**

33 One of the challenges in representing warm rain processes in global climate models  
34 (GCM) is related to the representation of the subgrid variability of cloud properties, such as cloud  
35 water and cloud droplet number concentration (CDNC), and the effect thereof on individual  
36 precipitation processes such as autoconversion. This effect is conventionally treated by  
37 multiplying the resolved-scale warm rain process rates by an enhancement factor ( $E_q$ ) which is  
38 derived from integrating over an assumed subgrid cloud water distribution. The assumed subgrid  
39 cloud distribution remain highly uncertain. In this study, we derive the subgrid variations of  
40 liquid-phase cloud properties over the tropical ocean using the satellite remote sensing products  
41 from Moderate Resolution Imaging Spectroradiometer (MODIS) and investigate the  
42 corresponding enhancement factors for the GCM parameterization of autoconversion rate. We  
43 find that the conventional approach of using only subgrid variability of cloud water is insufficient,  
44 and that the subgrid variability of CDNC, as well as the correlation between the two, are also  
45 important for the correctly simulating the autoconversion process in GCMs. Using the MODIS  
46 data which has the near-global data coverage, we find that  $E_q$  shows a strong dependence on  
47 cloud regimes, due to the fact that the subgrid variability of cloud water, and CDNC is regime-  
48 dependent. Our analysis shows a significant increase of  $E_q$  from the stratocumulus (Sc) to  
49 cumulus (Cu) regions. Furthermore, the enhancement factor  $E_N$  due to the subgrid variation of  
50 CDNC is derived from satellite observation for the first time, and results reveal several regions  
51 downwind of biomass burning aerosols (e.g., Gulf of Guinea, East Coast of South Africa), air  
52 pollution (i.e., Eastern China Sea), and active volcanos (e.g., Kilauea Hawaii and Ambae Vanuatu),  
53 where the  $E_N$  is comparable, or even larger than  $E_q$ , suggesting an important role of aerosol in  
54 influencing the  $E_N$ . MODIS observations suggest that the subgrid variations of cloud liquid water  
55 path (LWP) and CDNC are generally positively correlated. As a result, the combined enhancement  
56 factor, including the effect of LWP and CDNC correlation, is significantly smaller than the simple  
57 product of  $E_q \cdot E_N$ . Given the importance of warm rain processes in understanding the Earth  
58 system dynamics and water cycle, we conclude that more observational studies are needed to  
59 provide a better constraint on the warm rain processes in GCMs.

Formatted: Font: +Body (Calibri)

Deleted: difficulties of simulating the

Deleted: process

Deleted: how

Deleted: account for

Deleted: impact of

Deleted: variations

Deleted: ,

Deleted: the nonlinear

Deleted: In practice, this impact

Deleted: often

Deleted: adding a so-called

Deleted: term to the parameterization scheme

Deleted: MODIS (

Deleted: The wide spatial coverage

Deleted: product enables us to depict a detailed  
quantitative picture of the enhancement factor

Deleted: variation

Deleted: , which

Deleted: clear cloud regime dependence, namely a

Deleted: cloud

Deleted: Assuming a constant  $E_q = 3.2$  would  
overestimate the observed  $E_q$  in the Sc regions and  
underestimate it in the Cu regions. We also found that the  
 $E_q$  based on the Lognormal PDF assumption performs  
slightly better than that based on the Gamma PDF  
assumption. A simple parameterization scheme is provided  
to relate the  $E_q$  to the grid-mean liquid cloud fraction,  
which can be readily used in GCMs. For the first time

Deleted: even after the optically thin clouds are screened  
out. ...



## 1. Introduction

Marine boundary layer (MBL) clouds are a strong modulator of Earth's radiative energy budget (Klein and Hartmann, 1993; Trenberth et al., 2009). They can interact with other components of the climate system, such as aerosols and precipitations, in various ways. The feedback of MBL clouds to climate change remains one of the largest uncertainties in our understanding of the climate sensitivity (Bony and Dufresne, 2005; Soden and Held, 2006). Despite their importance in the climate system, simulating MBL clouds in general circulations models (GCM) has proved to be extremely challenging. A main difficulty is rooted in the fact the typical grid size of GCM (~100km) is much larger than the spatial scale of many cloud microphysical processes, and as a result these subgrid scale processes, as well as the subgrid cloud variations, have to be highly simplified and then parameterized as functions of resolved, grid-level variables.

Of particular interest in this study is the warm rain processes in MBL clouds, which have fundamental impacts on the cloud water budget and lifetime. Although in reality it is highly complicated and involves multiple factors, warm rain formation in GCMs is usually parameterized as simple functions of only key cloud parameters. For example, the drizzle in MBL cloud is initialized by the so-called autoconversion process in which the collision-coalescence of cloud droplets gives birth to large drizzle drops (Pruppacher and Klett, 1997). In GCMs, for the sake of efficiency, this process is usually parameterized as a power function of liquid water content (LWC or symbol  $q_c$ ) and cloud droplet number concentration (CDNC or symbol  $N_c$ ). One of the most widely used parameterization scheme is developed by Khairoutdinov and Kogan (2000) ("KK2000" hereafter), which has the form

$$\frac{\partial q_r}{\partial t} = C(q_c)^{\beta_q}(N_c)^{\beta_N} \quad (1)$$

where  $\frac{\partial q_r}{\partial t}$  is the rain water tendency due to the autoconversion process,  $q_c$  has the unit of kg/kg, and  $N_c$  of  $\text{cm}^{-3}$ . The three parameters  $C = 1350$ ,  $\beta_q = 2.47$  and  $\beta_N = -1.79$  are derived through a simple least-square fitting of the autoconversion rate results from a large-eddy simulation with bin microphysics that can simulate the process-level physics. Even though this is highly simplified, the parametrization scheme still faces a great challenge. The calculation of grid-

Deleted: ¶

Page Break

Deleted: Clouds

Deleted: (Klein and Hartmann, 1993; Trenberth et al., 2009)...

Deleted: ocean, land, and

Deleted: (Bony and Dufresne, 2005; Soden and Held, 2006)....

Deleted: conventional

Moved (insertion) [1]

Formatted: Indent: First line: 0"

Moved (insertion) [2]

Moved (insertion) [3]

Moved (insertion) [4]

mean autoconversion efficiency requires the knowledge of subgrid distributions of LWC and CDNC, but in the GCMs only grid-mean quantities  $\langle q_c \rangle$  and  $\langle N_c \rangle$  are known and available for use in the computation of autoconversion rate. As pointed out by Pincus and Klein (2000), for a process  $f(x)$  such as autoconversion that is nonlinearly dependent on subgrid variables,  $x$ , the grid-mean value  $\langle f(x) \rangle$  is not equal to the value estimated based on the grid-mean  $\langle x \rangle$ , i.e.,  $\langle f(x) \rangle \neq f(\langle x \rangle)$ . Mathematically, if  $f(x)$  is convex, then  $f(\langle x \rangle) < \langle f(x) \rangle$  (Larson and Griffin, 2013; Larson et al., 2001). To take this effect into account, a parameter  $E$  is often introduced in the GCM as part of the parameterization such that  $\langle f(x) \rangle = E \cdot f(\langle x \rangle)$ . It is referred to as the “enhancement factor” in many studies and this study too because  $E > 1$  for a convex function. Such a nonlinear effect is not just limited to the autoconversion process. Some other examples are the plane-parallel albedo bias (Barker, 1996; Cahalan et al., 1994; Oreopoulos and Davies, 1998a), subgrid cloud droplet activation (Morales and Nenes, 2010) and accretion (Boutle et al., 2014; Lebsock et al., 2013).

The value of  $E$  is determined primarily by two factors: the nonlinearity of  $f(x)$  and the subgrid probability density function (PDF)  $P(x)$ . Given the same subgrid variation of LWC, i.e.,  $P(q_c)$ , the nonlinear effect impacts the autoconversion parameterization more than it does on the accretion, because the former is a more nonlinear function of  $q_c$  than the latter. For the same  $f(x)$ , a grid box with a narrow and symmetric  $P(x)$  would require a smaller  $E$  than another grid box with a broader and non-symmetric  $P(x)$ . Ideally, the value of the enhancement factor  $E$  should be diagnosed from the subgrid cloud PDF  $P(x)$ . Unfortunately, because this is not possible in most conventional GCMs, the value of  $E$  is usually assumed to be a constant for the lack of better options. The  $E$  for autoconversion due to subgrid LWC variation is assumed to be 3.2 in the two-moment cloud microphysics parameterization schemes by Morrison and Gettelman (2008) (MG scheme hereafter), which is employed in the widely used Community Atmosphere Model (CAM). This choice of  $E = 3.2$  is based on an early study by Barker et al. (1996), in which the mesoscale variation of column-integrated optical thickness of the “overcast stratocumulus”, “broken stratocumulus” and “scattered stratocumulus” are studied. The value  $E = 3.2$  is derived based on the mesoscale variation of the broken stratocumulus.

**Moved (insertion) [5]**

**Moved (insertion) [6]**

**Moved (insertion) [7]**

**Deleted:** Of particular interest in this study is the warm rain processes in liquid-phase

**Moved up [1]:** clouds, which have fundamental impacts on the cloud water budget and lifetime. Although in reality it is highly complicated and involves multiple factors, warm rain formation in GCMs is usually parameterized as simple functions of only key cloud parameters.

**Deleted:** For example, the drizzle in MBL cloud is initialized by the so-called autoconversion process in which the collision-coalescence of cloud droplets gives birth to large drizzle drops (Pruppacher and Klett, 1997). In GCMs, for the sake of efficiency, this process is usually parameterized as a function of liquid water content (LWC or symbol  $q_c$ ) and cloud droplet number concentration (CDNC or symbol  $N_c$ ) (Khairoutdinov and Kogan, 2000) (see section 2 for details). Even though this is highly simplified, the parametrization scheme still faces a great difficulty

**Moved up [4]:** The calculation of grid-mean autoconversion efficiency requires the knowledge of subgrid distributions of LWC and CDNC, but in the GCMs only grid-mean quantities  $\langle q_c \rangle$  and  $\langle N_c \rangle$  are known and available for use in the computation of autoconversion rate.

**Deleted:** As pointed out by Pincus and Klein (2000)

**Moved up [5]:** , for a process  $f(x)$  such as autoconversion that is nonlinearly dependent on subgrid variables,  $x$ , the grid-mean value  $\langle f(x) \rangle$  is not equal to the value estimated based on the grid-mean  $\langle x \rangle$ , i.e.,  $\langle f(x) \rangle \neq f(\langle x \rangle)$ . Mathematically, if  $f(x)$  is convex, then  $f(\langle x \rangle) < \langle f(x) \rangle$

**Deleted:**  $\langle f(x) \rangle$  (Larson and Griffin, 2013; Larson et al., 2001)...

**Moved up [6]:** . To take this effect into account, a parameter  $E$  is often introduced in the GCM as part of the parameterization such that  $\langle f(x) \rangle = E \cdot f(\langle x \rangle)$ . It is referred to as the “enhancement factor” in many studies and this study too because  $E > 1$  for a convex function.

**Deleted:** Some other examples are the plane-parallel albedo bias (Barker, 1996; Cahalan et al., 1994; Oreopoulos et al., 1998a)

**Moved up [7]:** .

**Deleted:** process

**Deleted:** process

**Deleted:** The shape of the  $P(x)$  is dependent on mainly on cloud regime. Take cloud water for example. The subgrid

**Deleted:** , which should be scale aware and dependent on cloud regime....

**Deleted:** (2008)

**Deleted:** (1996)

Clearly, a simple constant  $E$  is not adequate. The following is a list of attempts to better understand the subgrid cloud variations and the implications for warm rain simulations in GCMs. Several previous studies have shown that the mesoscale cloud water variation is a strong function of cloud regime—the subgrid cloud water variation of Sc cloud is much different from that of Cu clouds (Barker et al., 1996; Lee et al., 2010; Oreopoulos and Cahalan, 2005; Wood and Hartmann, 2006). As the first part of a two-part study, Larson and Griffin (2013) first laid out a systematic theoretical basis for understanding the effects of subgrid cloud property variations on simulating various nonlinear processes in GCM, including not only the autoconversion but also the accretion, condensation, evaporation and sedimentation processes. In the second part, using cloud fields from a large-eddy simulation (LES), Griffin and Larson (2013) showed that inclusion of the enhancement factor indeed leads to more rainwater at surface in single-column simulations and makes them agree better with high-resolution large-eddy simulations. Using a combination of in situ measurement and satellite remote sensing data, Boutle et al. (2014) analyzed the spatial variation of both cloud and rain water, as well as their covariation, and developed a simple parameterization scheme to relate the subgrid cloud water variance to the grid-mean cloud fraction. Later, the study of Boutle et al. (2014) was extended by Hill et al. (2015) who developed a cloud regime dependent and scale-aware parameterization scheme for simulating subgrid cloud water variation. Recently, using the ground-based observations from three Department of Energy (DOE) Atmospheric Radiation Measurement (ARM) sites, Xie and Zhang (2015) developed a scale-aware parameterization scheme for GCMs to account for subgrid cloud water variation. Also using ARM measurement, Ahlgrimm and Forbes (2016) analyzed the dependence of cloud water variability on cloud regime. Although these previous studies have shed important light on subgrid cloud variation and the implications for GCM, they lack a global perspective because they are only based on limited data (e.g., LES cases, in situ and ground-based measurement). Currently, satellite remote sensing observation is the only way to achieve a global perspective. Using the observations from the space-borne radar CloudSat, Lebsock et al. (2013) showed that the subgrid cloud water variance is smaller over the Sc region than over the Cu region, and as a result the enhancement factor shows an increasing trend from Sc to Cu region. They also highlighted importance of considering the subgrid co-variability of cloud water and rain water in

**Deleted:** (Barker et al., 1996; Lee et al., 2010; Oreopoulos and Cahalan, 2005; Wood and Hartmann, 2006). As the first part of a two-part study, Larson and Griffin (2013) first laid out a systematic theoretical basis for understanding the effects of subgrid cloud property variations on simulating various nonlinear processes in GCM, including not only the autoconversion but also the accretion, condensation, evaporation and sedimentation processes. In the second part, using cloud fields from a large-eddy simulation (LES), Griffin and Larson (2013) showed that inclusion of the enhancement factor indeed leads to more rainwater at surface in single-column simulations and makes them agree better with high-resolution large-eddy simulations. Using a combination of in situ measurement and satellite remote sensing data, Boutle et al. (2014) analyzed the spatial variation of cloud and rain water, as well as their covariation. They further developed a simple parameterization scheme to relate the subgrid cloud water variance to the grid-mean cloud fraction. Recently, using the ground-based observations from three Department of Energy (DOE) Atmospheric Radiation Measurement (ARM) sites, Xie and Zhang (2015) developed a scale-aware parameterization scheme for GCMs to account for subgrid cloud water variation. Although these previous studies have shed important light on subgrid cloud variation and the implications for GCM, they lack a global perspective because they are only based on limited data (e.g., LES cases, in situ and ground-based measurement). Currently, satellite remote sensing observation is the only way to achieve a global perspective, although remote sensing products suffer from inherent retrieval uncertainties. Using the observations from the space-borne radar CloudSat, Lebsock et al. (2013) showed that the subgrid cloud water variance is larger over the Sc region than over the Cu region, and as a result the enhancement factor shows an increasing trend from Sc to Cu region. They also highlighted importance of considering the subgrid co-variability of cloud water and rain water in the computation of the accretion rate. On the modeling side, Guo et al. (2014) investigated the sensitivity of cloud simulation in the Geophysical Fluid Dynamics Laboratory (GFDL) Atmospheric General Circulation Model (AM) to the subgrid cloud water parameterization schemes. A similar study was carried out by Bogenschutz et al. (2013) using the National Center of Atmospheric Research (NCAR) Community Atmospheric Model (CAM). Both studies show that the more sophisticated subgrid parameterization scheme—Cloud Layers Unified by Binormals (CLUBB) (Golaz et al., 2002a; 2002b; Larson et al., 2002)—lead to a better simulation of clouds in the model. However, a more recent study by Song et al. (2017) reveals that the CLUBB in CAM version 5.3 (CAM5.3) overestimates the enhancement factor in the trade wind cumulus cloud region, which in turn leads to the “empty cloud” problem.

the computation of the accretion rate. On the modeling side, Guo et al. (2014) investigated the sensitivity of cloud simulation in the Geophysical Fluid Dynamics Laboratory (GFDL) Atmospheric General Circulation Model (AM) to the subgrid cloud water parameterization schemes. A similar study was carried out by Bogenschutz et al. (2013) using the National Center of Atmospheric Research (NCAR) Community Atmospheric Model (CAM). Both studies show that the more sophisticated subgrid parameterization scheme— Cloud Layers Unified by Binormals (CLUBB) (Golaz et al., 2002a; 2002b; Larson et al., 2002)—lead to a better simulation of clouds in the model. However, a more recent study by Song et al. (2018b) reveals that the CLUBB in CAM version 5.3 (CAM5.3) overestimates the enhancement factor in the trade wind cumulus cloud region, which in turn leads to excessive drizzle in the model and “empty clouds” with near-zero cloud water. In addition to CLUBB, the so-called super-parameterization (a.k.a Multiscale Modeling Framework (MMF)), which uses cloud resolving model embeded in the GCM grids to diagnose sub-grid cloud variations (Randall et al., 2003), have also gained increasing popularity. Takahashi et al. (2017) compared the subgrid cloud water variations simulated by a CAM-MMF model with those derived from A-Train observations and found reasonable agreement.

Despite these previous studies, many questions remain unanswered. First of all, all the previous studies, as far as we know, have focused on the impact of subgrid cloud water  $q_c$  variation. The potential impact of subgrid variation of  $N_c$  and the co-variability of  $N_c$  with  $q_c$  have been overlooked so far. Given the same amount of  $q_c$ , a cloud with a smaller  $N_c$  would have larger droplets and therefore larger precipitation efficiency than another cloud with a larger  $N_c$ . For the same reason, other things equal, a grid with positive correlation of subgrid  $N_c$  and  $q_c$  would be less efficient in terms of autoconversion than a grid with negative correlation of the two. Secondly, most of previous studies are based on the assumption that the subgrid cloud property variation follows certain well-behaved distributions, usually either Gamma (e.g., Barker, 1996; Morrison and Gettelman, 2008; Oreopoulos and Barker, 1999; Oreopoulos and Cahalan, 2005) or Lognormal (Boutle et al., 2014; Larson and Griffin, 2013; e.g., Lebsock et al., 2013). However, the validity and performance of the assumed PDF shape are seldom checked. Furthermore, although the study by Lebsock et al. (2013) has depicted a global picture of the

Formatted: Font color: Auto

**Deleted:** Despite these previous studies, many questions remain unanswered. First of all, all the previous studies, as far as we know, have focused on the impact of subgrid cloud water variation. The potential impact of subgrid variation of cloud microphysics, namely CDNC, has been overlooked so far. Given the same amount of cloud water, a cloud with a smaller CDNC would have larger droplets and therefore larger precipitation efficiency than another cloud with a larger CDNC. Secondly, most of previous studies are based on the assumption that the subgrid cloud property variation follows certain well-behaved distributions, usually either Gamma (e.g., Barker, 1996; Morrison and Gettelman, 2008; Oreopoulos and Barker, 1999; Oreopoulos and Cahalan, 2005) or Lognormal (Boutle et al., 2014; Larson and Griffin, 2013; e.g., Lebsock et al., 2013). However, the validity and performance of the assumed PDF shape are seldom checked. Furthermore, although the study by Lebsock et al. (2013) has depicted a global picture of the enhancement factor for the autoconversion modeling in GCM, the picture is far from clear due to the small sampling rate of CloudSat observations.

In this study, we revisit the subgrid variations of liquid-phase cloud properties over the tropical ocean using 10 years of MODIS cloud observations, with the overarching goal to better understand the potential impacts of subgrid cloud variations on the warm rain processes in the conventional GCMs. Similar to previous studies, we will quantify the subgrid cloud water variations based on MODIS observations. Going one step further, we will also attempt to unveil for the first time the subgrid CDNC variation and investigate its

enhancement factor for the autoconversion modeling in GCM, the picture is far from clear due to the small sampling rate of CloudSat observations.

In this study, we revisit the subgrid variations of liquid-phase cloud properties over the tropical ocean using 10 years of MODIS cloud observations, with the overarching goal to better understand the potential impacts of subgrid cloud variations on the warm rain processes in the conventional GCMs. Similar to previous studies, we will quantify the subgrid cloud water variations based on MODIS observations. Going one step further, we will also attempt to unveil for the first time the subgrid  $N_c$  variation, as well as its correlation with cloud water, and investigate the implications for warm rain simulations in GCM. Moreover, we will take advantage of the wide spatial coverage of MODIS data to achieve a more detailed picture of the enhancement factor for the autoconversion simulation. Last but not least, we will evaluate the two widely used distributions, i.e., Lognormal and Gamma, in terms of their performance and limitations for simulating the enhancement factor. We will first explain the theoretical background in Section 2 and introduce the data and methodology in Section 3. The MODIS observations will be presented and discussed in Section 4. The implications for the autoconversion parameterization in the GCMs will be discussed in 5. The main findings will be summarized in Section 6 with an outlook for future studies.

## 2. Theoretical Background

### 2.1. Theoretical Distributions to describe subgrid cloud property variations

In previous studies, the spatial variations of cloud properties, such as cloud optical thickness (COT), cloud liquid water path (LWP) and cloud liquid water content (LWC), are often described using either of two theoretical distributions—the Gamma and Lognormal distribution. The probability density function (PDF) from a Gamma distribution is a two-parameter function as follows (Barker, 1996; Oreopoulos and Davies, 1998b):

$$P_G(x) = \frac{1}{\Gamma(v)} \alpha^v x^{v-1} \exp(-\alpha x), \quad (2)$$

where  $\Gamma$  is the Gamma function,  $v$  is the so-called inverse relative variance, and  $\alpha$  the so-called rate parameter. If  $x$  follows the Gamma distribution, its mean value is given by

**Deleted:** ¶  
The rest of the paper is organized as follows, we

**Deleted:** of the grid mean values and subgrid variations of key cloud properties

**Deleted:** process simulation

**Field Code Changed**

**Deleted:** The mean value of a

$$\langle x \rangle = \int_0^{\infty} x P_G(x) dx = \frac{v}{\alpha}, \quad (3)$$

and variance given by

$$Var(x) = \int_0^{\infty} (x - \langle x \rangle)^2 P_G(x) dx = \frac{v}{\alpha^2}. \quad (4)$$

It follows from Eq. (3) and (4) that the so-called inverse relative variance is

$$v = \frac{1}{\eta} = \frac{\langle x \rangle^2}{Var(x)}, \quad (5)$$

where  $\eta = \frac{Var(x)}{\langle x \rangle^2}$  is the relative variance. If  $x$  follows the Gamma distribution, for a physical process  $M(x)$  that is a power function of  $x$ ,

$$M(x) = Kx^\beta, \quad (6)$$

then the expected value  $\langle M(x) \rangle$  is given by

$$\langle M(x) \rangle_G = K \int_0^{\infty} x^\beta P_G(x) dx = \frac{\Gamma(v+\beta)}{\Gamma(v)v^\beta} K \langle x \rangle^\beta, \quad \beta > -v. \quad (7)$$

As explained in the introduction, for a nonlinear process  $M(x)$ ,  $\langle M(x) \rangle \neq M(\langle x \rangle)$ . The ratio between the two  $E$  is by definition the enhancement factor:

$$E(P_G, v, \beta) = \frac{\langle Kx^\beta \rangle}{K \langle x \rangle^\beta} = \frac{1}{\langle x \rangle^\beta} \int_0^{\infty} x^\beta P_G(x) dx = \frac{\Gamma(v+\beta)}{\Gamma(v)v^\beta}. \quad (8)$$

The PDF of a Lognormal distribution is given as follows (Larson and Griffin, 2013; Lebsack et al., 2013):

$$P_L(x) = \frac{1}{\sqrt{2\pi}x\sigma} \exp\left(-\frac{(\ln x - \mu)^2}{2\sigma^2}\right), \quad (9)$$

where  $\mu = \langle \ln x \rangle$  and  $\sigma^2 = Var(\ln x)$  correspond to the mean and variance of  $\ln x$ , respectively.

The mean value of the Lognormal distribution is given by

$$\langle x \rangle = \int_0^{\infty} x P_L(x) dx = e^{\mu + \frac{\sigma^2}{2}}, \quad (10)$$

and the variance by

$$Var(x) = \int_0^{\infty} (x - \langle x \rangle)^2 P_L(x) dx = e^{2\mu + \sigma^2} (e^{\sigma^2} - 1). \quad (11)$$

It follows from Eq. (10) and (11) that the inverse relative variance can be derived from the following equation

Deleted: the

Formatted: Indent: First line: 0"

Deleted: ¶  
The PDF of a Lognormal

Deleted: given as follows (Larson and Griffin, 2013; Lebsack et al., 2013):

Formatted Table

Deleted:  $P_L(x) = \frac{1}{\sqrt{2\pi}x\sigma} \exp\left(-\frac{(\ln x - \mu)^2}{2\sigma^2}\right)$ ,

Deleted: are the two parameters that determine the shape of the Lognormal distribution and

Formatted: Justified

Deleted: given



$$e^{\sigma^2} = 1 + \frac{Var(x)}{\langle x \rangle^2} = 1 + \frac{1}{v}. \quad (12)$$

If  $x$  follows the Lognormal distribution, the expected value of  $\langle M(x) \rangle$  is

$$\langle M(x) \rangle_L = K \int_0^\infty x^\beta P_L(x) dx = \left(1 + \frac{1}{v}\right)^{\frac{\beta^2 - \beta}{2}} K \langle x \rangle^\beta. \quad (13)$$

Evidently, the corresponding enhancement factor is given by

$$E(P_L, v, \beta) = \frac{\langle K x^\beta \rangle}{K \langle x \rangle^\beta} = \left(1 + \frac{1}{v}\right)^{\frac{\beta^2 - \beta}{2}}. \quad (14)$$

Note that Eq. (7) and (8) are only valid when  $\beta > -v$  because Gamma function  $\Gamma(v + \beta)$  can run into singular values when  $v + \beta < 0$ . In contrast, Eq. (13) and (14) are valid for any real value  $\beta$ . This is one advantage of the Lognormal distribution over the Gamma distribution.

An example of the Gamma and Lognormal distributions for  $q_c$  is shown in Figure 1a. In this example, both distributions have the same mean  $\langle q_c \rangle = 0.5 \text{ g/kg}$  and also the same inverse relative variance  $v_q = 3$ . Although the general shapes of the two PDFs are similar, they differ significantly at the two ends: the Gamma PDF is larger than Lognormal PDF over the small values of  $q_c$ , and the opposite is true over the large values of  $q_c$ . The Gamma and Lognormal distributions can also be used to describe the spatial variation of  $N_c$  (Gultepe and Isaac, 2004). An example is given in Figure 1c, in which  $q_c$  is a constant of  $0.5 \text{ g/kg}$ ,  $\langle N_c \rangle = 50 \text{ cm}^{-3}$ , and  $v_N = 5.0$ .

Figure 1b shows the autoconversion rate based on the KK2000 parameterization scheme for the Gamma  $P_G(q_c)$  and Lognormal  $P_L(q_c)$  that are shown in Figure 1a. Interestingly, although the cumulative autoconversion rates based on the two types of PDFs are almost identical, the contribution to the total autoconversion rate from the different LWC bins are quite different. As show in Figure 1a, the  $P_L(q_c)$  has a longer tail than the  $P_G(q_c)$ , i.e., the occurrence probability of large  $q_c$  (e.g.,  $q_c > 2.0 \text{ g/kg}$ ) is much higher in the Lognormal than in Gamma PDF. This difference is further amplified in the autoconversion rate computation in Figure 1b because the autoconversion rate is proportional to  $q_c^{2.47}$ .

The enhancement factors based on the Gamma (i.e.,  $E(P_G, \beta)$  in Eq. (8)) and Lognormal (i.e.,  $E(P_L, \beta)$  in Eq. (14)) PDF for  $\beta_q = 2.47$  are plotted as a function of the inverse relative variance  $v$  in Figure 2. When subgrid clouds are more homogenous i.e.,  $v > 1$ , the enhancement

Moved (insertion) [8]

Moved (insertion) [9]

Moved (insertion) [10]

Moved (insertion) [11]

Deleted: LWC

Deleted:  $\langle LWC \rangle =$

Deleted:  $v =$

Deleted: LWC,

Deleted: LWC.

Deleted: CDNC

Deleted: (Gultepe and Isaac, 2004).

Deleted: the LWC=

Deleted: the mean CDNC

Deleted: and the inverse relative variance of CDNC  $v =$

Deleted: ¶

Both Gamma and Lognormal distributions are mathematically convenient. For example, if any physical process  $M(x)$  is a power function of  $x$ , ¶ ... [3]

Moved up [8]:  $x$  follows the Lognormal distribution, the expected value of  $\langle M(x) \rangle$  is ¶

Deleted: ¶

$$\langle M(x) \rangle_L = K \int_0^\infty x^\beta P_L(x) dx = \left(e^{\sigma^2}\right)^{\frac{\beta^2 - \beta}{2}} K \langle x \rangle^\beta. \quad \dots [4]$$

Deleted: expected value

Deleted:  $\langle M(x) \rangle$  can be computed

Moved (insertion) [12]

Deleted: analytical solutions above, instead

Moved (insertion) [13]

Deleted: a numerical integration over the

Deleted: However, it is important to note that Eq. (10) is only valid when  $\beta > -v$ . The

Moved up [9]: Gamma function  $\Gamma(v + \beta)$  can run into singular values when  $v + \beta < 0$ . In contrast, Eq.

Moved up [10]: In contrast, Eq.

Deleted: (11)

Moved (insertion) [14]

Moved (insertion) [15]

Moved (insertion) [16]

Moved (insertion) [17]

factor based on the two PDFs are similar. However, for more inhomogeneous grids with i.e.,  $\nu < 1$ , the  $E(P_L, \beta)$  is significantly larger than that  $E(P_G, \beta)$ , which is probably because of the longer tail of  $P_L(q_c)$  as shown in Figure 1 a and b.

## 2.2. Impacts of subgrid cloud variations on warm rain parameterization in GCM

The warm rain process in MBL clouds involves many interacting microphysical processes. In this study, we only focus only on the simulation of autoconversion in GCM. Other nonlinear processes, such as accretion and evaporation have been investigated in previous studies (Boutle et al., 2014; Lebsock et al., 2013).

Ideally, if the subgrid variations of  $q_c$  and  $N_c$  are known, then the grid-mean in-cloud autoconversion rate should be derived from the following integral

$$\left\langle \frac{\partial q_r}{\partial t} \right\rangle = \int_0^\infty \int_0^\infty C(q_c)^{\beta_q} (N_c)^{\beta_N} P(q_c, N_c) dq_c dN_c, \quad (15)$$

where  $P(q_c, N_c)$  is the joint PDF of  $q_c$  and  $N_c$ . Unfortunately, most conventional GCMs lack the capability of predicting the subgrid variations of cloud properties, with only a couple of exceptions (Thayer-Calder et al., 2015). What is known from the GCM is usually the in-cloud grid-mean values  $\langle q_c \rangle$  and  $\langle N_c \rangle$ . As a result, instead of using Eq. (15), the autoconversion rate in GCMs is usually computed from the following equation

$$\left\langle \frac{\partial q_r}{\partial t} \right\rangle = E \cdot C(\langle q_c \rangle)^{\beta_q} (\langle N_c \rangle)^{\beta_N}, \quad (16)$$

where  $E$  is the enhancement factor defined as:

$$E = \frac{\int_0^\infty \int_0^\infty (q_c)^{\beta_q} (N_c)^{\beta_N} P(q_c, N_c) dq_c dN_c}{(\langle q_c \rangle)^{\beta_q} (\langle N_c \rangle)^{\beta_N}} \quad (17)$$

The value of the enhancement factor depends on the subgrid variations of  $q_c$  and  $N_c$ . If clouds are homogenous on the subgrid scale, then  $E \sim 1$ . The more inhomogeneous the clouds are, the larger the  $E$  is. In the special case where  $q_c$  and  $N_c$  are independent, then the joint PDF  $P(q_c, N_c)$  becomes  $P(q_c, N_c) = P(q_c)P(N_c)$ , where  $P(q_c)$  and  $P(N_c)$  are the PDF of the subgrid  $q_c$  and  $N_c$ . Consequently, Eq. (15) reduces to

$$\left\langle \frac{\partial q_r}{\partial t} \right\rangle = C \int_0^\infty (q_c)^{\beta_q} P(q_c) dq_c \int_0^\infty (N_c)^{\beta_N} P(N_c) dN_c. \quad (18)$$

**Moved up [11]:** This is one advantage of the Lognormal distribution over the Gamma distribution. [1]

**Deleted:** valid for any real value  $\beta$ .

**Deleted:** simulations

**Deleted:** climate models

**Moved (insertion) [18]**

**Deleted:** As pointed out in Pincus and Klein (2000), the subgrid cloud property variations have important implications for modeling the nonlinear cloud processes in climate models, such as the precipitation and radiative transfer processes. Of particular interest to this study is the auto-conversion process that initializes the warm rain in marine boundary layer clouds. Following Khairoutdinov and Kogan (2000) ("KK2000" hereafter), the auto-conversion rate is often modeled in GCMs as a power function of LWC and cloud droplet number concentration (CDNC) as follows [1]

**Moved (insertion) [19]**

**Deleted:**  $\frac{\partial q_r}{\partial t} = C(q_c)^{\beta_q} (N_c)^{\beta_N}$ ,

**Moved (insertion) [20]**

**Moved (insertion) [21]**

**Moved (insertion) [22]**

**Deleted:** where  $\frac{\partial q_r}{\partial t}$  is the rain water tendency due to the auto-conversion process,  $q_c$  is the cloud water mixing ratio in the unit of kg/kg,  $N_c$  is the CDNC in the unit

**Moved up [2]:** of  $\text{cm}^{-3}$ . The three parameters

**Moved up [3]:** The three parameters  $C = 1350$ ,  $\beta_q = 2.47$  and  $\beta_N = -1.79$  are derived through a

**Moved up [18]:** Ideally, if the subgrid variations of  $q_c$

**Deleted:** least-square fitting of the rain rate results from a large-eddy simulation. The KK2000 scheme has been adopted in the popular two-moment cloud microphysics [5]

**Deleted:** and  $N_c$  are known, then the grid-mean in-cloud [6]

**Moved (insertion) [23]**

**Moved up [19]:**  $\left\langle \frac{\partial q_r}{\partial t} \right\rangle =$

**Moved up [20]:** where  $P(q_c, N_c)$  is the joint PDF of  $q_c$

**Deleted:** Unfortunately, most conventional GCMs lack the [7]

**Moved up [21]:** What is known from the GCM is usually

**Moved up [22]:** and  $\langle N_c \rangle$ . As a result, instead of using

**Deleted:** (13), the auto-conversion rate in GCMs is usually [8]

**Moved up [23]:**  $\left\langle \frac{\partial q_r}{\partial t} \right\rangle = E \cdot C(\langle q_c \rangle)^{\beta_q} (\langle N_c \rangle)^{\beta_N}$ ,

**Deleted:** where  $E$  is referred to as the "enhancement" [9]

**Formatted:** Line spacing: 1.5 lines

**Commented [VL2]:** I doubt that this is often true in [10]

and Eq.(17), to

$$E = E_q \cdot E_N, \quad (19)$$

where  $E_q$  is the enhancement factor due to the subgrid variation of cloud water which has the form,

$$E_q = \frac{\int_0^\infty (q_c)^{\beta_q} P(q_c) dq_c}{(\langle q_c \rangle)^{\beta_q}} \quad (20)$$

and the  $E_N$  is the enhancement factor due to the subgrid variation of  $N_c$  which has the form,

$$E_N = \frac{\int_0^\infty (N_c)^{\beta_N} P(N_c) dN_c}{(\langle N_c \rangle)^{\beta_N}} \quad (21)$$

Obviously, if  $P(q_c)$  and  $P(N_c)$  follow either Gamma or Lognormal distribution, then the above equations reduce to Eq. (8) or (14), respectively.

If  $q_c$  and  $N_c$  both have significant subgrid variations and they are not independent, the enhancement factor should ideally be diagnosed from Eq. (17). However, the joint PDF  $P(q_c, N_c)$  may not be known and the integration can be time-consuming. Some previous studies proposed to approximate the  $P(q_c, N_c)$  as a bivariate lognormal distribution as follows:

$$P(q_c, N_c) = \frac{1}{2\pi q_c N_c \sigma_q \sigma_N \sqrt{1 - \rho^2}} \exp\left(-\frac{\zeta}{2}\right) \quad (22)$$

$$\zeta = \frac{1}{1 - \rho^2} \left[ \left( \frac{\ln q_c - \mu_q}{\sigma_q} \right)^2 - 2\rho \left( \frac{\ln q_c - \mu_q}{\sigma_q} \right) \left( \frac{\ln N_c - \mu_N}{\sigma_N} \right) + \left( \frac{\ln N_c - \mu_N}{\sigma_N} \right)^2 \right],$$

where  $\rho$  is the correlation coefficient between  $q_c$  and  $N_c$  (Larson and Griffin, 2013; Lebsock et al., 2013). As such, both  $q_c$  and  $N_c$  follow a marginal lognormal distribution in Eq. (9). Substituting Eq. (22) into Eq. (17), we obtain the enhancement factor for the bivariate lognormal distribution that consists of three terms

$$E = E_q(P_L, v_q, \beta_q) \cdot E_N(P_L, v_N, \beta_N) \cdot E_{COV}(\rho, \beta_q, \beta_N, v_q, v_N) \quad (23)$$

where  $E_q(P_L, v_q, \beta_q) = \left(1 + \frac{1}{v_q}\right)^{\frac{\beta_q^2 - \beta_q}{2}}$  and  $E_N(P_L, v_N, \beta_N) = \left(1 + \frac{1}{v_N}\right)^{\frac{\beta_N^2 - \beta_N}{2}}$  correspond to the impacts of subgrid  $q_c$  and  $N_c$  variance, respectively (i.e., Eq. (14)), and the third term

$$E_{COV}(\rho, \beta_q, \beta_N, v_q, v_N) = \exp(\rho \beta_q \beta_N \sigma_q \sigma_N) \quad (24)$$

Deleted: And

Deleted: reduces

Deleted:  $E_q = \frac{\int_0^\infty \int_0^\infty (q_c)^{\beta_q} P(q_c) dq_c}{(\langle q_c \rangle)^{\beta_q}}$ ,

Deleted:  $E_q$

Deleted: cloud water

Deleted:  $E_N = \frac{\int_0^\infty \int_0^\infty (N_c)^{\beta_N} P(N_c) dN_c}{(\langle N_c \rangle)^{\beta_N}}$ .

corresponds to the impact of the co-variation of  $q_c$  and  $N_c$  on the enhancement factor. Obviously, Eq. (23) reduces to Eq. (19) when  $q_c$  and  $N_c$  are uncorrelated (i.e.,  $\rho = 0$ ,  $E_{COV} = 1$ ). If  $q_c$  and  $N_c$  are negatively correlated (i.e.,  $\rho < 0$  and  $E_{COV} > 1$ ), clouds with larger  $q_c$  would tend to have smaller  $N_c$ . The autoconversion rate in such a case would be larger than that in the case where  $q_c$  and  $N_c$  are positively correlated (i.e., i.e.,  $\rho > 0$  and  $E_{COV} < 1$ ). A positive correlation would exist, for instance, if all droplets in cloud were the same size, but some parcels had more droplets than other parcels.

Most current GCMs do not have the capability to simulate the subgrid cloud property variations. They usually have to use pre-defined subgrid cloud variations in the computation of grid-mean autoconversion rate instead of using prognostic values. For example, in the MG scheme for the CAM5.3, the subgrid  $q_c$  is assumed to follow the Gamma distribution in Eq. (2) with a fixed  $v_q = 1$  and as a result constant  $E_q = 3.2$ . Lately, advanced subgrid parameterization schemes, such as CLUBB, have been implemented in several GCMs, including CAM6 and GFDL AM model (Bogenschutz et al., 2017; Guo et al., 2015; 2014), which provides information on the subgrid  $q_c$  variation to the host model. The information can then be used to dynamically diagnose the enhancement factor  $E_q$ , which will help the model simulate the cloud regime dependence of  $E_q$  (Guo et al., 2010; 2014).

However, as explained above, not only the subgrid variation of  $q_c$  but the subgrid variation of  $N_c$  can also influence the enhancement factor. Unfortunately, this aspect has been ignored by almost all GCMs, even the latest CAM6 with CLUBB. Physically, provided the same  $q_c$ , a cloud with smaller  $N_c$  would have larger droplet size and therefore larger precipitation efficiency than the cloud with larger  $N_c$ . Because the autoconversion rate depends nonlinearly on  $N_c$ , the grid-mean autoconversion rate computed based on a skewed PDF of  $N_c$  (i.e.,  $\int_0^\infty (N_c)^{\beta_N} P(N_c) dN_c$ ) would be different from that computed based on the mean of  $N_c$  (i.e.,  $\langle N_c \rangle^{\beta_N}$ ). The autoconversion enhancement factor based on the Lognormal PDF  $E(P_L, \beta)$  for  $\beta_N = -1.79$  is given in Figure 2. Interestingly, at the same inverse relative variance  $v$ , the enhancement factor based on the same Lognormal PDF  $E(P_L, \beta)$  for  $\beta_N = -1.79$  is actually larger than that for  $\beta_q = 2.47$  because of the formula of the exponent in Eq. (14) (i.e.,  $\frac{\beta^2 - \beta}{2}$ ). Moreover, the correlation between  $N_c$  and  $q_c$  can also be important. Going back to Eq. (23),

Moved (insertion) [24]

Moved (insertion) [25]

Moved down [26]: is assumed to follow the Gamma distribution in Eq. (1)

Deleted: ¶

Because most current GCMs do not have the capability to simulate the subgrid cloud property variations, models usually use pre-defined subgrid cloud variations in the computation of grid-mean auto-conversion rate instead of using prognostic values. For example, in the MG scheme for the CAM5.3, the subgrid LWC

Deleted: (1). Furthermore, it is assumed that the subgrid variation of CDNC is small and therefore the enhancement factor due to CDNC variation is negligible (i.e., close to unity). Substituting the Gamma distribution in Eq. (1) into the definition equation of enhancement factor in Eq. (18), and with help from Eq. (10), one can derive that ¶ ... [11]

Moved up [12]: As show in Figure 1a, the  $P_L(q_c)$  has a longer tail than the  $P_G(q_c)$ , i.e., the occurrence probability

Moved up [13]: (e.g.,  $q_c > 2.0g/kg$ ) is much higher in the Lognormal than in Gamma

Moved (insertion) [27]

Deleted: PDF. This difference is further amplified in the rain rate computation in Figure 1b because the rain rate is proportional to  $q_c^{2.47}$ . ¶

Moved up [14]: The enhancement factors based on the Gamma (i.e.,  $E(P_G, \beta)$ ) in Eq.

Moved up [15]:  $E(P_L, \beta)$  in Eq.

Moved up [16]: ) PDF for  $\beta_q = 2.47$  are plotted as a function of the inverse relative variance  $v$  in Figure 2. When

Deleted: of large LWC

Deleted: (20)) and Lognormal (i.e.,

Deleted: (21)

Moved up [17]: When subgrid clouds are more homogenous i.e.,  $v > 1$ , the enhancement factor based on the two PDFs are similar. However, for more inhomogeneous grids with i.e.,  $v < 1$ , the  $E(P_L, \beta)$  is significantly larger than that  $E(P_G, \beta)$ , which is probably

Moved (insertion) [26]

Deleted: It is important to note that

Formatted: Indent: First line: 0.5"

Deleted: can lead to a nonlinear effect on the simulation of autoconversion rate,

Deleted: can have the same effect.

Deleted: LWC,

Deleted: (i.e.,  $\frac{\beta^2 - \beta}{2}$ ). This potentially important effect of ... [12]

evidently,  $E > E_q$  if and only if  $E_N \cdot E_{COV} > 1$ . After some manipulation, we can show that if  $\beta_N < 0$  and  $\sigma_N > 0$ , then

$$E_N \cdot E_{COV} > 1, \text{ if } \rho < \frac{\sigma_N}{\sigma_q} \cdot \frac{(1-\beta_N)}{2\beta_q} \quad [25]$$

This equation reveals that when  $q_c$  and  $N_c$  are weakly or negatively correlated ( $\rho \leq 0$ ), considering only  $E_q$  would tend to underestimate  $E$ . On the other hand, however, if  $q_c$  and  $N_c$  are highly positively correlated ( $\rho \sim 1$ ) then considering  $E_q$  only would tend to overestimate  $E$ .

### 3. Data and Methodology

To derive the above-mentioned enhancement factors, we will use 10 years (2007 ~ 2016) of the latest collection 6 (C6) *daily mean* level-3 cloud retrieval product from the Aqua-MODIS instrument (product name “MYD08 D3”), which contains the gridded statistics of cloud properties computed from pixel-level (i.e., level-2) retrievals. As summarized in Platnick et al. (2003; 2017), the operational level-2 MODIS cloud product provides cloud masking (Ackerman et al., 1998), cloud top height (Menzel et al., 1983), cloud top thermodynamic phase determination (Menzel et al., 2006), and COT, cloud effective radius (CER) and LWP retrievals based on the bi-spectral solar reflectance method (Nakajima and King, 1990). All MODIS level-2 atmosphere products, including the cloud, aerosol and water vapor products, are aggregated to  $1^\circ \times 1^\circ$  spatial resolution on a daily, eight-day, and monthly basis. Aggregations include a variety of scalar statistical information, including mean, standard deviation, max/min occurrences, as well as histograms including both marginal and joint histograms. For COT, CER and LWP, the MODIS level-3 product provides both their “in-cloud” grid-mean values ( $\langle x \rangle$ ) and subgrid standard deviations ( $\sigma_x$ ). The inverse relative variance  $v$  can then be derived from Eq. (5), i.e.,  $v = \langle x \rangle^2 / \sigma_x^2$ . Note that the operational MODIS product provides two CER retrievals, one based on the observation from the band 7 centered around  $2.1 \mu\text{m}$  and the other from band 20 at  $3.7 \mu\text{m}$ . As discussed in several previous studies (Cho et al., 2015; Zhang and Platnick, 2011; Zhang et al., 2012; 2016), the  $3.7 \mu\text{m}$  band CER retrieval is more resilient to the 3-D effects and retrieval failure than the  $2.1 \mu\text{m}$  band retrievals. For these reasons, it is used as the observational reference in this study.

Given the COT and CER retrieval, the operational MODIS product estimates the LWP of cloud

**Deleted:** Finally, it has to be noted that when both  $q_c$  and  $N_c$  have significant subgrid variations, their covariation also becomes important. As explained in Griffin and Larson (2013), if the  $q_c$  and  $N_c$  are negatively correlated,

**Moved up [24]:** clouds with larger  $q_c$  would tend to have smaller  $N_c$ . The autoconversion rate in such a case

**Moved up [25]:** The autoconversion rate in such a case would be larger than that in the case where  $q_c$  and  $N_c$  are positively correlated (i.e.,

**Deleted:** larger  $q_c$  would tend to have larger  $N_c$ ). As explained in Eq. (17), only when they are uncorrelated can the total enhancement factor be decomposed into the product of two independent factors  $E = E_q \cdot E_N$ . Otherwise additional terms are necessary to take into account the effect of  $q_c$  and  $N_c$  correlation. Although potentially important, the correlation of  $q_c$  and  $N_c$  from satellite remote sensing data is difficult to derive from the satellite remote sensing observations due to the retrieval uncertainties. We will return to this point later in Section 5.3.

**Moved (insertion) [28]**

**Deleted:** Of particular interest to this study are the grid-mean value and subgrid variation of several key properties of liquid-phase clouds, namely, COT, CER, LWP and CDNC, in the tropical regions. For this purpose, we use the latest collection 6 (C6) *daily mean* level-3 cloud retrieval product from the Aqua-MODIS instrument (product name “MYD08 D3”). The MODIS level-3 (i.e., grid-level) product contains statistics computed from a set of level-2 (

**Moved up [27]:** i.e.,

**Deleted:** pixel-level) MODIS granules. As summarized in (Platnick et al., 2003; 2017), the operational level-2 MODIS cloud product provides cloud masking (Ackerman et al., 1998), cloud top height (Menzel et al., 1983), cloud top thermodynamic phase determination (Menzel et al., 2006), and COT, CER and LWP retrievals based on the bi-spectral solar reflectance method (Nakajima and King, 1990)

**Moved up [28]:** All MODIS level-2 atmosphere products, including the cloud, aerosol and water vapor products, are aggregated to  $1^\circ \times 1^\circ$  spatial resolution on a daily, eight-day, and monthly basis. Aggregations include a variety of scalar statistical information, including mean, standard deviation, max/min occurrences, as well as histograms including both marginal and joint histograms. For COT, CER and LWP, the MODIS level-3 product provides both their “in-cloud” grid-mean values ( $\langle x \rangle$ ) and subgrid standard deviations ( $\sigma_x$ ).

**Deleted:** The inverse relative variance  $v$  can then be derived from Eq. ...

**Deleted:** , i.e.,  $v = \langle x \rangle^2 / \sigma_x^2$ . Note that the operational MODIS product provides two CER retrievals, one based on the observation from the band 7 centered around  $2.1 \mu\text{m}$  and the other from band 20 at  $3.7 \mu\text{m}$ . As discussed in ... [13]

using

$$LWP = \frac{2}{3} \rho_w COT \cdot CER, \quad (26)$$

where  $\rho_w$  is the density of water. Several studies have argued that a smaller coefficient of 5/9, instead of 2/3, should be used in estimation of LWP (Lebsock et al., 2011; Seethala and Horváth, 2010; Wood and Hartmann, 2006). The choice of coefficient does not matter in this study because it is a common factor in the calculation of  $v$ . The choice of the coefficient has no impact on our study, because we are interested in the relative inverse variance  $v = \langle x \rangle^2 / \sigma_x^2$ . We note here that it is the LWC,  $q_{CL}$ , instead of the LWP, that is used in the KK2000 scheme. So, the spatial variability of LWC is what is most relevant. However, the remote sensing of cloud water vertical profile from satellite sensor for liquid-phase clouds is extremely challenging even with active sensors. It is why most previous studies using the satellite observations analyzed the spatial variation of LWP, rather than LWC. In fact, even Lebsock et al. (2013), who used the level-2 CloudSat observations, had to use the vertical averaged LWC in their analysis. Airborne in situ measurement faces similar challenge. For example, Boutle et al. (2014) use the LWC observation along “horizontal flight tracks” to study the spatial variability of cloud water, which only samples the LWC at certain levels of MBL clouds. Ground-based observations are much better than satellite and airborne observation in this regard. Recently, Xie and Zhang (2015) analyzed the cloud water profiles retrieved using ground-based radars from the three ARM sites and found no obvious in-cloud vertical dependence of the spatial variability of LWC. Following these previous studies, we assume that the horizontal subgrid variation of LWC is *not* strongly dependent on height and its value can be inferred from the spatial variability of the vertical integrated quantity LWP. The uncertainty caused by this assumption will be assessed in future studies.

The current MODIS level-3 cloud product does *not* provide CDNC retrievals. Following previous studies (Bennartz, 2007; Bennartz and Rausch, 2017; Grosvenor and Wood, 2014; McCoy et al., 2017a), we estimate  $N_c$  of liquid-phase clouds from the MODIS retrieved COT ( $\tau$ ) and CER ( $r_e$ ) based on the classic adiabatic cloud model

**Deleted:** (Seethala and Horváth, 2010; Wood and Hartmann, 2006)....

**Deleted:** ,

**Deleted:** Ground-based observations are much better than satellite observation in this regard because they are closer to the target (i.e. clouds).

**Deleted:** Following previous studies (Bennartz, 2007; Bennartz and Rausch, 2017; Grosvenor and Wood, 2014; McCoy et al., 2017a), we estimate the CDNC ( $N_c$ )



$$N_c(\tau, r_e) = \frac{\sqrt{5}}{2\pi k} \frac{\sqrt{f_{ad}\Gamma_w}}{\sqrt{\rho_w Q_e}} \tau^{\frac{1}{2}} r_e^{-\frac{5}{2}} = \frac{\sqrt{15}}{2\pi k} \frac{\sqrt{f_{ad}\Gamma_w}}{\rho_w \sqrt{2Q_e}} LWP^{\frac{1}{2}} r_e^{-3}, \quad (27)$$

Deleted: ,

where  $\rho_w$  is the density of water;  $Q_e \approx 2$  is the extinction efficiency of cloud droplets;  $k$  is the ratio of  $r_e$  to mean volume-equivalent radius;  $f_{ad}$  is the adiabaticity of the cloud;  $\Gamma_w$  is the LWC lapse rate. Following previous studies, we assume  $k = 0.8$  and  $f_{ad} = 1.0$  to be constant and compute  $\Gamma_w$  from the grid mean liquid cloud top temperature and pressure. The theoretical basis and main uncertainty sources of the CDNC estimation based on the adiabatic cloud model from MODIS-like passive cloud retrievals are nicely reviewed by Grosvenor et al. (2018).

Commented [VL13]: Does it work for cumulus clouds?

Commented [zz14R13]: For cumulus clouds, the adiabaticity is less than 1.0 which can lead to error on CDNC retrieval. However, because we are more concerned with the relative variance, the error in the denominator will cancel the error in the nominator.

Deleted: (2018)

Ideally, the values of LWP and CDNC should be estimated on pixel-by-pixel basis from the level-2 MODIS product. However, pixel-by-pixel estimation is highly time consuming, which makes it difficult to achieve a global perspective. Using an alternative method, many previous studies estimate the grid-level CDNC statistics from the joint histogram of COT vs. CER provided in the level-3 MODIS cloud products (Bennartz, 2007; McCoy et al., 2017a; 2017b). For a given  $1^\circ \times 1^\circ$  grid-box, the liquid-phase COT-CER joint histogram provides the counts of successful cloud property retrievals with respect to 108 joint COT-CER bins that are bounded by 13 COT bin boundaries, ranging from 0 to 150, and 10 CER bin boundaries, ranging from  $4 \mu\text{m}$  to  $30 \mu\text{m}$ . With the joint histogram, which is essentially the joint PDF of COT and CER  $P(\tau, r_e)$ , we can estimate the grid mean and variance of CDNC from the following equations

Field Code Changed

$$\langle x \rangle = \int \int x(\tau, r_e) P(\tau, r_e) d\tau dr_e, \quad (28)$$

$$Var(x) = \int \int (x(\tau, r_e) - \langle N_c \rangle)^2 P(\tau, r_e) d\tau dr_e, \quad (29)$$

where  $x$  can be either LWP or CDNC. Figure 3a shows the LWP in Eq. (26) as a function of the 13 COT bins and 10 CER bins from the MODIS level-3 product. As expected, the largest LWP values are found when both COT and CER are large. Figure 3b shows the CDNC in Eq. (27) as a function of the COT and CER bins. As expected, the largest CDNC values are found when both COT is large and CER is small. Figure 3c shows an example of the COT-CER joint histogram from the Aqua-MODIS daily level-3 product "MYD08\_D3" on January 09<sup>th</sup>, 2007 at the grid box  $1^\circ\text{S}$  and  $1^\circ\text{W}$ . In this particular grid box, a combination of  $\sim 2\text{--}4$  COT and  $\sim 10\text{--}12 \mu\text{m}$  CER is the most frequently

Deleted: ~

Deleted:  $\mu\text{m}$  ~

827 observed cloud value. Using the joint histogram in Figure 3c, we can derive the mean and variance  
828 of both LWP and COT using the Eqs. (28) and (29).

829 The efficiency of using the level-3 MODIS product is accompanied by three important  
830 limitations. First of all, as mentioned earlier MODIS provides only LWP retrievals while LWC is  
831 needed in the KK2000 scheme. Second, the current level-3 MODIS cloud product has a fixed 1°x1°  
832 spatial resolution. Although this resolution is highly relevant to the current generation of GCMs,  
833 i.e., Coupled Model Intercomparison Project Phase 6 (CMIP5) (Eyring et al., 2016), future GCMs  
834 may have significantly finer resolution. Third, it is difficult to sub-sample the pixels with the best  
835 retrieval quality. These limitations will have to be addressed in future studies.

#### 836 4. Grid-mean and subgrid variations of liquid-phase cloud properties

837 In this study, we limit our analysis to tropical oceans only where warm rain is frequent and  
838 MODIS cloud retrievals have a relatively better quality than over land or over high latitude. The  
839 annual mean total cloud fraction ( $f_{tot}$ ), liquid-phase cloud fraction ( $f_{liq}$ ), in-cloud COT, CER from  
840 the 3.7  $\mu\text{m}$  band, LWP and estimated CDNC over the tropical oceans based on 10 years Aqua-  
841 MODIS retrievals are shown in Figure 4. The highest  $f_{liq}$  in the tropics is usually found in the  
842 stratocumulus (Sc) decks over the Eastern boundary of the ocean, e.g., SE Pacific off coast of Peru,  
843 NE Pacific off the coast of California and SE Atlantic off the coast of Namibia. The liquid-cloud  
844 fraction reduces significantly toward the open ocean trade wind regions, where the dominant  
845 cloud types are broken cumulus (Cu). Close to the continents, the Sc decks are susceptible to the  
846 influence of continental air mass with higher loading of aerosols in comparison with pristine  
847 ocean environment, which is probably the reason the SC decks have smaller CER and higher CDNC  
848 than the open-ocean trade cumulus (Figure 4 d and f). The in-cloud COT (Figure 4 c) and LWP  
849 (Figure 4 e) generally increase from the Sc decks to the open-ocean Cu regime, although less  
850 dramatically than the transition of cloud fraction. The Sc decks and the Sc-to-Cu transition are  
851 the most prominent features of liquid-phase clouds in the tropics. However, as mentioned in the  
852 introduction, simulating these features in the GCMs proves to be an extremely challenging task,  
853 and most GCMs suffer from some common problems, such as the “too few too bright” problem  
854 and the abrupt Sc-to-Cu transition problem (Kubar et al., 2014; Nam et al., 2012; Song et al.,  
855 2018a).

**Deleted:** The efficiency of using the level-3 product is accompanied by two important limitations. First, the current level-3 MODIS cloud product has a fixed 1°x1° spatial resolution. Although this resolution is highly relevant to the current generation of GCMs, i.e., CMIP5 (Taylor et al., 2012), future GCMs may have significantly finer resolution. Second, it is difficult to sub-sample the pixels with the best retrieval quality. As reviewed in Grosvenor et al. (2018), the main source of uncertainty in the CDNC retrieval is the MODIS retrieval uncertainties, particularly in CER because of

$N_c \sim r_e^{-5/2}$  dependence. In the pixel-by-pixel method, the pixel-level retrieval uncertainties, as well as some other metrics such as the sub-pixel inhomogeneity index, provided in the level-2 product can be used to select the pixels with the best retrieval quality. Here, because we use the static COT-CER joint histogram provided in the operational level-3 product, we do not have the flexibility to sub-sample the data using retrieval quality. Alternatively, we can sub-sample the data using the COT. It is well known that the bi-spectral retrieval method has a large uncertainty for thin clouds. Indeed, the clouds with COT thinner than about 4 have often been screened out in previous studies (Quaas et al., 2008). Such screening can be easily done with the joint PDF of COT and CER, but it would obviously lead to sampling bias in LWP. The impact on CDNC is dependent on whether the CDNC is correlated with the COT, i.e., whether thin clouds have the similar CDNC as the thick clouds. We will revisit this point later. It should be noted that because thin clouds in MODIS retrieval tend to have large uncertainty, any type of data quality-based data screening would inevitably lead to the sampling bias. ¶

**Commented [VL15]:** Within-cloud average or grid-box average?

**Deleted:** These regions are associated with relatively low sea surface temperature (SST) due to cold upwelling ocean surface current and mid-tropospheric subsidence of warm air from large-scale circulations, which together lead to a strong low-tropospheric stability and high liquid-cloud fraction. With an annual mean TOA cloud radiative effect usually around  $-40 \sim -60 \text{ W/m}^2$ , the Sc decks are important modulators of the local and global radiative energy budget.

**Deleted:** dominate

**Field Code Changed**

**Formatted:** Font color: Auto

**Deleted:** 2018

**Formatted:** Font color: Auto

Switching the focus now from grid-mean values to subgrid variability, we will show the grid-level inverse relative variances  $v = \langle x \rangle^2 / \text{Var}(x)$  for several key cloud properties. Here, we first derive the daily mean  $v$  and then aggregate the result to monthly mean values. Therefore, for each grid box we have 120 samples (i.e., 10 years x 12 months) of monthly mean  $v$  for analysis and visualization. Because the value of  $v$  can be ill-behaved when  $\text{Var}(x)$  approaches zero, instead of the mean value, we plot the median value of  $v$  based on 120 months of MODIS observations in Figure 5. There are several interesting and important features in Figure 5. First of all, the  $v$  of all four sets of cloud properties (i.e., COT, CER, LWP and CDNC) all exhibits a clear and similar Sc-to-Cu transition, with larger values in the Sc region and smaller value in the broken Cu regions. This indicates that cloud properties, including both optical and microphysical properties, are more homogenous, in terms of spatial distribution within the grid, in the Sc region than in the Cu region. Secondly, the value of  $v$  of CER (i.e., 10~100 in Figure 5b) is larger than that of the other properties (i.e., 1~10) by almost an order of magnitude, indicating that the subgrid variability of CER is very small. On the other hand, however, it is important to note that the  $v$  of CDNC (Figure 5d) is comparable with that of COT (Figure 5a) and LWP (Figure 5c). The reason is probably in part because the highly nonlinear relationship between CDNC and CER (i.e.,  $N_c \sim r_e^{-\frac{5}{2}}$ ) leads to a stronger variability of CDNC than CER, and also in part because the variability of CDNC is also contributed by the subgrid variation of COT. In some regions, the Gulf of Guinea, East and South China Sea, and Bay of Bengal for example, the  $v$  of CDNC is close to unity, indicating the subgrid standard deviation of CDNC is comparable to the grid-mean values in these regions. As discussed in the next section, the significant subgrid variability of CDNC in these regions should be taken into account when modeling the nonlinear processes, such as the autoconversion, in GCM to avoid systematic biases due to the nonlinearity effect.

The values of  $v$  in Figure 5 from this study are in reasonable agreement with previous studies. Barker (1996) selected a few dozens of cloud scenes, each about 100 ~ 200 km in size, from the Landsat observation and analyzed their spatial variability of COT. It is found that the typical value of  $v$  for “overcast stratocumulus”, “broken stratocumulus” and “scattered cumulus” is 7.9, 1.2, and 0.7, respectively (see their Table 3), which is consistent with the Sc-to-Cu transition pattern seen in Figure 5. Oreopoulos and Cahalan (2005) derived the subgrid inhomogeneity of

**Deleted:** Recall that  $v$  is defined such that the larger the  $v$ , the larger the mean value in comparison with the variance, and the more homogeneous the cloud property within the grid....

**Deleted:** 10 years

**Deleted:** auto-conversion

**Deleted:** Barker (1996)

**Deleted:** Oreopoulos and Cahalan (2005)

934 COT on a global scale from the level-3 Terra-MODIS retrievals. Although using a different metric  
 935 (i.e., their inhomogeneity parameter is defined as  $\chi = \exp(\ln\langle\tau\rangle) / \langle\tau\rangle$ ), they also found  
 936 systematic increase of inhomogeneity (decreasing value of  $\chi$ ) from the Sc region to cu region.  
 937 Also using the MODIS cloud property retrievals, Wood and Hartmann(2006) investigated the  
 938 meso-scale spatial variability of LWP in the NE Pacific and SE Pacific region. The  $\nu$  of LWP is found  
 939 to increase systematically with meso-scale cloud fraction and the relationship between the two  
 940 can be reasonably explained by a simple PDF cloud thickness model in Considine et al. (1997).  
 941 See also Kawai and Teixeira (2010).

Deleted: (2006)

Deleted: (1997).

Deleted: (2010)

942 As explained in section 2, the correlation between cloud water and CDNC can also  
 943 influence the computation of enhancement factor and thereby the grid-mean autoconversion  
 944 rate. Figure 5e shows the median value of the LWP and CDNC correlation coefficient  $\rho$ . Similar to  
 945 the derivation of median  $\nu$ , we first compute the monthly mean  $\rho$  from daily MODIS observations  
 946 and then derive the median value of  $\rho$  for each grid from the 120 months of observation. As  
 947 shown in Figure 5e, at the subgrid level, the LWP and CDNC tend to be positively correlated  
 948 almost over all tropical oceans. Mathematically, this is not surprising because as shown in Figure  
 949 5b and c, the subgrid variability of  $r_e$  is order of magnitude smaller than that of LWP. Since CDNC  
 950 is proportional to  $LWP^{\frac{1}{2}} r_e^{-3}$  according to Eq. (27), the subgrid variability of CDNC is mainly  
 951 determined by the variability of LWP, leading to the positive correlation. Physically, the  
 952 correlation can be explained by several mechanisms. For example, Wood et al. {\*Wood:2018cx}  
 953 and O et al. {\*O:2018to} found that a large amount of low-level water clouds over the  
 954 stratocumulus to cumulus transition are “optically thin veil clouds”. These clouds are usually  
 955 associated with low LWP and low CDNC (therefore positive correlation) and probably caused by  
 956 the strong precipitation scavenging process in the active cumulus. Note that our definition of  $\rho$  is  
 957 the subgrid spatial correlation of LWP and CDNC. It may be different from the definition used in  
 958 many aerosol indirect effect studies where the temporal correlation of monthly mean LWP and  
 959 CDNC is more interested.

## 5. Implications for warm-rain simulations in GCM

### 5.1. Influence of subgrid variation of cloud water

As discussed in Section 2.2, most current GCMs only considers the impact of subgrid cloud water variation on autoconversion rate but ignore the impact of subgrid CDNC variation. To make our analysis relevant to the current GCMs, we first analyze  $E_q$  in Eq. (20) based on observation. The impacts of subgrid CDNC variation (i.e.,  $E_N$ ) and its correlation with cloud water (i.e.,  $E_{COV}$ ) will be analyzed in the next section.

We derive  $E_q$  using two approaches. First, we derive it from the observed LWP PDF based on Eq. (20). As such, we do not have to make any assumption about the shape of LWP PDF although solving the integration in Eq. (20) is time-consuming. In the second approach, we first derive the relative inverse relative variance  $v$  of LWP and then derive the enhancement factor by assuming the subgrid PDF to be either Gamma or Lognormal. This approach is more efficient, but it may be subject to error if the true PDF deviates from the assumed PDF shape. Figure 6a shows the annual mean enhancement factor  $E_q$  in the tropical region derived based on Eq. (20) (i.e., the first approach) from 10 years of MODIS observation. Figure 6 b and c show the annual mean enhancement factor  $E_q$  derived by assuming the subgrid cloud water follows the Lognormal (i.e., Eq. (14)) and Gamma distribution (i.e., Eq. (8)), respectively. There are a couple of interesting and important points to note. First of all, similar to the grid-mean quantities in Figure 4, the enhancement factor  $E_q$  also shows a clear Sc-to-Cu transition. Over the Sc decks, because clouds are more homogeneous ( $v > 5$ ), the enhancement factor  $E_q$  is only around  $1 \sim 2.5$ , while over the Cu regions, the more inhomogeneous clouds with  $v < 1$  leads to a larger enhancement factor  $E_q$  around  $3 \sim 5$ . As aforementioned, in the current CAM5.3,  $E_q$  is assumed to be a constant of 3.2. While this value is within the observational range, it obviously cannot capture the Sc-to-Cu transition. In fact, the constant value 3.2 overestimates the  $E_q$  over the Sc region and underestimates the  $E_q$  over the Cu region, which could lead to unrealistic drizzle production in both regions and to consequential impacts on cloud water budget, radiation and even aerosol indirect effects on the model. The second point to note is that the  $E_q$  based on the Lognormal PDF assumption in Figure 6 b agrees well with the results in Figure 6 a derived directly from the observation. In contrast, the  $E_q$  based on the Gamma PDF assumption in Figure 6 c tends to be

Deleted: LWP ¶

As explained in the Theoretical Background, in GCMs the influences of subgrid cloud water variability on the simulation of highly nonlinear autoconversion process are accounted for using the enhancement factors defined...

Formatted: Heading 2, Left, Outline numbered + Level: 2 + Numbering Style: 1, 2, 3, ... + Start at: 1 + Alignment: Left + Aligned at: 0.25" + Indent at: 0.55"

Moved down [29]: in Eq.

Deleted: (15). For example, in CAM5.3, the MG cloud microphysics parameterization scheme assumes that the subgrid cloud water follows the Gamma distribution with the value of  $v = 1$ , which leads to a constant enhancement factor of 3.2 for the KK2000 autoconversion scheme (Morrison and Gettelman, 2008). Because its direct connection with the precipitation rate, the enhancement factor can have significant impacts on precipitation, cloud, and radiation fields of the host model. For the same reason, it is also often used as a "tuning" parameter to optimize the model and reduce the differences between model simulations and observations (Guo et al., 2014). Thus ¶

Moved (insertion) [29]

Deleted: given the subgrid cloud property variations, ¶

Deleted: the enhancement factor

Deleted: In the first

Deleted: can

Deleted: the enhancement factor based on its definition ¶

Deleted: PDF of LWP or CDNC, respectively. The ... [17]

Formatted: Indent: First line: 0.25"

Deleted: the subgrid cloud property variation (i.e., ... [18]

Deleted: this approach is more

Deleted:

Deleted: because it has to solve the integration.

Deleted: (i.e., Eq. (20)) or Lognormal (i.e., using Eq. (21)).

Deleted: although

Deleted: significant

Deleted: ¶

Deleted: median

Deleted: median

Deleted: ,

Deleted: product

Deleted: b

Deleted: tend

1071 smaller, especially in the Cu regions. This result seems to suggest that the Lognormal distribution  
 1072 provides a better fit to the observed subgrid cloud water variation than the Gamma distribution,  
 1073 which has rarely been noted and reported in the previous studies.

1074 A flexible, cloud-regime dependent  $E_q$  could help improve the simulation of Sc-to-Cu  
 1075 transition in the GCM. If a GCM employs an advanced cloud parameterization scheme, such as  
 1076 CLUBB, that is able to provide regime-dependent information on subgrid cloud variation, i.e.,  $v$ ,  
 1077 then the enhancement factor  $E_q$  could be diagnosed from  $v$ . However, most traditional cloud  
 1078 parameterization schemes do not provide information on subgrid cloud variation. In such case, if  
 1079 one does not wish to use a constant  $E_q$ , but a varying regime-dependent scheme, then either  $v$   
 1080 or  $E_q$  need to be parameterized as a function of some grid-mean cloud properties resolved by  
 1081 the GCM. In [fact](#), several attempts have been made along this line. Based on the combination air-  
 1082 borne in situ measurement and satellite remote sensing product, Boutle et al. [\(2014\)](#)  
 1083 parameterized the “fractional standard deviation” (which is equivalent to  $1/\sqrt{v}$  in our definition)  
 1084 of liquid-phase cloud as a function of grid-mean cloud fraction. This scheme was later updated  
 1085 and tested in a host GCM in Hill et al. [\(2015\)](#), and was found to reduce the shortwave cloud  
 1086 radiative forcing biases in the model. In a recent study, Xie and Zhang [\(2015\)](#) derived the subgrid  
 1087 cloud variations from the ground-based observations from three Department of Energy (DOE)  
 1088 Atmospheric Radiation Measurement (ARM) sites, and then parameterize the inverse relative  
 1089 variance  $v$  as a function of the atmospheric stability.

1090 Figure 7a shows the variation of inverse relative variance  $v$  as a function of the grid-mean  
 1091 liquid-phase cloud fraction  $f_{liq}$ . In general, the value of  $v$  increases with the increasing  $f_{liq}$ , which  
 1092 is expected from the Sc-to-Cu increase of  $f_{liq}$  in Figure 4b and the Sc-to-Cu decrease of  $v$  in Figure  
 1093 5c. The  $v(f_{liq})$  pattern in Figure 7a [is also consistent with the results reported in Wood and](#)  
 1094 [Hartmann \(2006\) and Lebsock et al. \(2013\). In the hope of obtaining a simple parameterization](#)  
 1095 [scheme for  \$v\(f\_{liq}\)\$  that can be used in GCMs, we fit the median value of  \$v\$  as a simple 3<sup>rd</sup> order](#)  
 1096 polynomial of  $f_{liq}$  as follows:

$$v(f_{liq}) = 2.38 - 4.95f_{liq} + 8.74f_{liq}^2 - 0.49f_{liq}^3, \quad f_{liq} \in [0, 1]. \quad (30)$$

Commented [V16]: I wonder if Robin Hogan has ever compared lognormal and gamma PDFs, for ice or radar reflectivity at least.

Deleted: facts

Deleted: (2014)

Deleted: (2015)

Deleted: (2015)

Deleted: a is also consistent with the results reported in Wood and Hartmann (2006) and Lebsock et al. (2013). In the hope of obtaining a simple parameterization scheme for  $v(f_{liq})$  that can be used in GCMs, we fit the median value of

Deleted:  $\in$  (

1106 To test the performance of this simple parameterization, we first substitute the  $f_{liq}$  from MODIS  
 1107 daily mean level-3 product into the above equation and then use the resultant  $v$  to compute the  
 1108 enhancement factor  $E_q$ . Unfortunately, the enhancement factor  $E_q$  computed based on the  
 1109 parameterized  $v(f_{liq})$  as shown in Figure 8a substantially underestimate the observation-based  
 1110 results in Figure 6, especially over the Cu regions. The deviation is probably because the  
 1111 relationship between  $E_q$  and  $v$  is highly nonlinear (e.g., Eq. (8) and (14)) and therefore the above  
 1112 parameterization scheme that only fits the  $\bar{v}$  value of  $v$  is not able to capture the variability of  
 1113  $E_q$ . Based on this consideration, we tried an alternative approach. Instead of parameterization  
 1114 of  $v$ , we directly parameterize the enhancement factor  $E_q$  as a function of  $f_{liq}$ . Figure 7b shows  
 1115 the variation of  $E_q$  as a function of  $f_{liq}$ . As expected,  $E_q$  generally decreases with increasing  $f_{liq}$ .  
 1116 The median value of  $E_q$  is fitted with the following 3<sup>rd</sup> order polynomial of  $f_{liq}$

$$E_q(f_{liq}) = 2.72 + 7.33f_{liq} - 19.17f_{liq}^2 + 10.69f_{liq}^3, \quad f_{liq} \in [0, 1]. \quad (31)$$

1117 As shown in Figure 8b, the value of  $E_q$  based on the above equation clearly agrees with the  
 1118 observation-based values in Figure 6 better than that based on the parameterization of  $v(f_{liq})$ .  
 1119 The elimination of the middle step indeed improves the parameterization results. While this is  
 1120 encouraging, it should be kept in mind that the Eq. (31) has very limited application, i.e., it is only  
 1121 useful for the autoconversion rate computation for a particular value of the autoconversion  
 1122 exponent beta, i.e.,  $\beta_q = 2.47$ . A good parameterization of  $v$  could be useful for not only  
 1123 autoconversion, but also for accretion and radiation computations. Another caution is that, if  
 1124 applied to a GCM, the performance of the  $E_q(f_{liq})$  parameterization in Eq. (31) will be dependent  
 1125 on the simulated accuracy of  $f_{liq}$  in the model.

## 1127 5.2. Influence of subgrid variance of CDNC

1128 Now we will investigate the impacts of subgrid CDNC variation on the autoconversion rate  
 1129 simulation. For the moment, we will consider  $E_N$  only. The impact of CDNC and cloud water  
 1130 correlation will be discussed in the next section. Similar to  $E_q$ , we first derive  $E_N$  from the CDNC  
 1131 PDF based on Eq. (21). The annual mean result based on 10 years of MODIS observations is shown  
 1132 in Figure 9a. There are several intriguing points to note. First of all, the value of  $E_N$  is actually

Deleted: the median value of

Deleted: median

Deleted:  $\in$  (

Deleted: median

Commented [V17]: What value of the autoconversion exponent was assumed here?

Deleted: . In future study, we will implement this parameterization scheme in a couple of GCMs and study the impacts on the cloud, precipitation and radiation simulations. We will also explore better ways to parameterize the inverse relative variance  $v$

Deleted: In

Deleted: previous section, we have mainly focused on the enhancement factor  $E_q$  on autoconversion simulation due to the ...

Deleted: of cloud water. In this section

Deleted: switch the focus on the enhancement factor

Deleted: due to the subgrid variation

Deleted: . ¶  
The median value of

Deleted: derived

Deleted: from

Deleted: observation



larger than  $E_q$  in Figure 9 such that we even have to use a different color scale for this plot. Secondly,  $E_N$  the regions with escalated  $E_N$  seem to coincide with the downwind regions of biomass burning aerosols (e.g., Gulf of Guinea, East Coast of South Africa), air pollution (i.e., Eastern China Sea), and, most interestingly, active volcanos (e.g., Kilauea Hawaii and Ambae Vanuatu). We have also checked the seasonal variation of the  $E_N$  and the results also support this observation. Another interesting feature to note is that, although the dust outflow regions such as Tropical East Atlantic and Arabian Sea, have heavy aerosol loading, the value of  $E_N$  there is only moderate. Figure 9b shows the value of  $E_N$  computed based on Eq. (14) from the inverse relative variance of  $v$ , assuming that the subgrid CDNC follows a Lognormal PDF. Although the overall pattern is consistent with Figure 9a, the assumption of Lognormal PDF seems to underestimate  $E_N$ . A closer examination indicates that the Lognormal PDF tend to underestimate the population of clouds with small CDNC, and therefore underestimate the variance of CDNC as well as  $E_N$ . We did not compute the  $E_N$  based on the Gamma distribution because of the singular value problem aforementioned in Section 2.1.

We could not find any previous observation-based study on the global pattern of the subgrid variation of CDNC and the corresponding  $E_N$ . So, it is difficult for us to corroborate our results. On one hand, the magnitude of  $E_N$  is surprisingly large. As explained in Section 3, the CDNC is estimated based on Eq. (27) from the MODIS retrieval of COT and CER. Several previous studies have shown that the sub-pixel level surface contamination, subpixel cloud inhomogeneity, and three-dimensional radiative transfer effects, can cause significant errors in the MODIS CER retrievals especially over broken cloud regions (Zhang and Platnick, 2011; Zhang et al., 2012; 2016). Given the fact that the CDNC retrieval is highly sensitive to CER error as a result of  $N_d \sim r_e^{-\frac{5}{2}}$ , the influence of retrieval uncertainty on subgrid CDNC variation cannot be ruled out. On the other hand, the pattern of  $E_N$  in Figure 9a seems to suggest that there are some underlying physical mechanisms controlling the subgrid variation of CDNC, in which aerosols seem to play an important role. To achieve a better understanding, we analyzed the dependence of  $E_N$  on liquid cloud fraction and grid-mean CDNC in Figure 10, which reveals that  $E_N$  has a stronger dependence on CDNC than cloud fraction. This result seems to indicate that the pattern of  $E_N$  in Figure 9 is largely determined by physical mechanisms rather than retrieval

**Commented [V18]:** Importantly (and confusingly),  $E_N$  is small in the main Sc regions off the coasts of California, Peru, and Namibia. Why aren't there variations in  $N_c$  in those regions off the coasts? Autoconversion will be not be enhanced in those regions by variations in  $N_c$  (or  $q_c$ ).

To me, it looks like  $E_N$  is controlled by variations in the (remote) source of aerosol, whereas  $E_Q$  is controlled by variability in cumulus clouds that is locally induced by turbulence. But neither is large in Sc.

Is it possible that the high values of  $E_N$  are an artifact of time variability in the aerosol as a plume of pollution from, e.g., a fire, meanders across the ocean? Is there such large variability in instantaneous snapshots? Can the MODIS observations work on instantaneous data instead of time averages?

**Commented [zz19R18]:** These are very good questions. I don't have clear answers at the moment. Some small scale CDNC variation is due to retrieval artifacts. But as shown later, even we screen out the COT<5 data, the results are still similar.

I'm in favor of your hypothesis about the spatial variation of  $E_N$ . In this paper, I just want to hold on the "observation" and leave the in-depth study of the causes to future work.

**Deleted:** (shown in supplementary materials)

**Commented [V20]:** How accurate is the gamma distribution?

**Deleted:**

**Commented [V21]:** It might be reassuring to compare with aircraft observations. Do any aircraft observations show CER varying from 4 to 30 microns?

**Commented [zz22R21]:** Yes, in situ measurement would be highly useful. But it will be left for future work.

**Deleted:** . On one hand, the pattern of  $E_N$  in Figure 9a seems to suggest that there are some underlying physical mechanisms controlling the subgrid variation of CDNC, in which aerosols seem to play an important role. On the other hand, the magnitude of  $E_N$  is surprisingly large. As explained in section 3, the CDNC is estimated based on Eq. (23) from the MODIS retrieval of COT and CER. Could retrieval uncertainty contribute to the large subgrid variation of CDNC and therefore  $E_N$ ? In order to better understand the large value of  $E_N$ , we selected a case during the biomass burning season in the Gulf of Guinea, which is shown in Figure 10. During the boreal winter, the grassland and savanna fires in the southern West Africa generate a thick layer of smoke aerosols that are clearly visible in the satellite image (Andreae and Merlet, 2001). On this day, the Gulf of Guinea is quite cloudy, filled with broken cumulus clouds in the northern coastal region and stratiform clouds in the south. We arbitrarily selected a smaller region, marked with the red box, for detailed analysis. Although the cloud fraction in this region is about 60%, the clouds are [19]

uncertainties. Interestingly, the largest  $E_N$  is usually found when liquid cloud fraction is small and CDNC is large and decreases with decreasing CDNC and increasing cloud fraction. This pattern leads us to the following hypothesis: In the regions where aerosol is limited, even weak updraft can activate most cloud condensation nuclei (CCN). As a result, even if there is significant subgrid variation of turbulence at cloud base, the subgrid variation of CDNC remains small. In contrast, in regions where aerosol is abundant, the subgrid variation of turbulence becomes important. The subgrid variation of updraft leads to subgrid variation CDNC and thereby large  $E_N$ .

As far as we know, the results in Figure 9 and Figure 10 mark the first attempt based on satellite observations to unveil the global pattern of the subgrid variations of CDNC and investigate the consequential impacts on warm rain simulations in GCMs. Although obscured by satellite retrieval uncertainties, the results still provide valuable insights. First of all, the enhancement factor  $E_N$  due to the subgrid variations of CDNC is nonnegligible, even comparable the effect of subgrid cloud water variation (i.e.,  $E_q$ ). Second, the global pattern of  $E_N$  in Figure 9 provides a valuable map for future studies.

### 5.3. The combined effect of subgrid variations of cloud water and CDNC

Finally, in this section we examine the combined effect of subgrid variations of cloud water and CDNC, as well as their correlation, on the autoconversion rate simulation. The annual mean combined enhancement factor  $E$  derived based on Eq. (17) from 10 years of MODIS COT and CER observation is shown in Figure 11a. Comparing to the  $E_q$  in Figure 6 and  $E_N$  in Figure 9, the combined enhancement factor is generally larger. It is easy to see that in some regions (e.g., Gulf of Guinea, East Coast of South Africa and Eastern China Sea) the combined enhancement factor  $E$  resembles the  $E_N$  while in other regions (i.e., trade wind cumulus regions over open ocean) it resembles more of  $E_q$ . Interestingly, because both  $E_q$  and  $E_N$  are small over the Sc decks, those regions have the smallest combined enhancement factor  $E$ . As discussed in Section 2.2, only when the subgrid variation of cloud water is uncorrelated with the subgrid variation of CDNC can the combined enhancement factor  $E$  be decomposed into the simple product of  $E_q$  and  $E_N$  (i.e., Eq. (19)). Figure 11b shows the annual mean value of the simple product  $E_q \cdot E_N$ , without considering the correlation between cloud water and CDNC. Evidently, the simple product substantially overestimates the combined enhancement factor derived from

**Deleted:** The results from the above case study raises some concerns. It seems that the large variations of CER and therefore CDNC are usually associated with thin clouds. While there could be a physical explanation (e.g., CCN activation), it seems more likely to be caused, or at least contributed, by retrieval uncertainty. It is well known that the bispectral method has large uncertainties for thin clouds, especially when they are broken. Several previous studies have shown that the sub-pixel level surface contamination, subpixel inhomogeneity, and three-dimensional radiative transfer effects, tend to cause overestimated CER retrieval on top of large uncertainties (Zhang and Platnick, 2011; Zhang et al., 2012; 2016). Therefore, for such a challenging case in Figure 10, it is not surprising that the large CDNC variation and  $E_N$  are partly caused by retrieval uncertainty. Based on this consideration, we did a sensitivity test, in which we screen out the thin clouds with COT < 4 in the computation and analysis of CDNC and  $E_N$ . The result from this test is shown in Figure 9c. Indeed, the removal of thin clouds substantially reduces the value of  $E_N$ . For example, in the Gulf of Guinea, the median value of  $E_N$  reduces by a factor of 4 from about 10 to only about 2.5. Nevertheless, the global pattern of  $E_N$  still remains, i.e., nonnegligible values of  $E_N$  are found in the downwind regions of biomass burning, air pollution and volcano emission. ¶

**Deleted:** Figure 10

**Deleted:** several

**Deleted:** , which in our opinion should focus on the regions with large  $E_N$ , e.g., Gulf of Guinea, East Coast of South Africa and Eastern China Sea. Last, but not least, the example in Figure 10 clearly exposes the limitation of the current satellite remote sensing method. There are alternative methods for retrieving the CDNC from satellite [20]

**Deleted:** As discussed in Section 2.2,

**Deleted:** the

**Deleted:** can be derived from joint PDF  $P(q, N_c)$  based on Eq. (15). Because both  $q$  and  $N_c$  are a function of the retrieved COT and CER, we can easily derive the

**Deleted:** from the COT-CER joint histogram of MODIS product simply changing the integration domain of Eq.

**Deleted:** from  $q$  and  $N_c$  to COT and CER. The median value of the combined enhancement factor  $E$  based on Eq. (15)...

**Deleted:** As one would expect,

**Deleted:** than both  $E_q$  in Figure 6 and the  $E_N$  in Figure 9.

**Deleted:** ¶

**Deleted:** ). Otherwise, additional terms that could be quite complicated are needed to account for the effect of correlation (Lebsock et al., 2013). Here, we performed a couple of simple tests to understand the potential ... [21]

the joint PDF of LWP and CDNC. This result can be explained by the mostly positive subgrid correlation between LWP and CDNC in Figure 5e. As explained in section 2.2, the positive correlation means that clouds with more water also tend to have more CDNC. The autoconversion rate of such configuration is lower than that when LWP and CDNC have no correlation.

Together, the  $E_q$  in Figure 6,  $E_N$  in Figure 9 and the combined enhancement factor in Figure 11 lead us to the following important conclusion. It is not sufficient to consider only the impact of subgrid variation of cloud water (i.e.,  $E_q$ ) on the autoconversion rate simulation. The influences of subgrid CDNC variation, as well as the correlation between cloud water and CDNC, must also be taken into account to avoid significant error.

Finally, the combined enhancement factor derived based on Eq. (23) assuming that the LWP and CDNC follow the bi-variate lognormal distribution is shown in Figure 11c. Despite the tendency of overestimation, the result agrees reasonably well with that based on observed joint PDF in Figure 11a, clearly better than the simple product  $E_q \cdot E_N$ . This is encouraging as it suggests that the bi-variate lognormal distribution can be used in the future to model the combined effect of cloud water and CDNC on autoconversion rate simulation in GCMs.

## 6. Summary and Outlook

One of the difficulties in GCM simulation of the warm rain parameterization is how to account for the impact of subgrid variations of cloud properties, such as cloud water and CDNC, on nonlinear precipitation processes such as autoconversion. In practice, this impact is often treated by adding the enhancement factor term to the parameterization scheme. In this study, we derived the subgrid variations of liquid-phase cloud properties over the tropical ocean using the satellite remote sensing products from MODIS and investigated the corresponding enhancement factors for parameterizations of autoconversion rate. In comparison with previous work, our study is able to shed some new light on this problem in the following regards:

1. A theoretical framework is presented to explain the importance of the subgrid variation of CDNC and its correlation with cloud water on the autoconversion rate simulation in GCMs.

Moved down [30]: (i.e.,

Formatted: Font: Times New Roman

Deleted: optically thin clouds with less cloud water tend to have larger CER and smaller CDNC). This correlation mainly exists among optically thin clouds as a result of retrieval bias and uncertainty and it tends to counteract the effect of  $E_q$  and  $E_N$  making the combined enhancement factor  $E$  substantially smaller than the simple product of  $E_q \cdot E_N$  (i.e., assuming no correlation).

Deleted: process

2. The wide spatial coverage of the Level-3 MODIS product enables us to depict a detailed quantitative picture of the enhancement factor  $E_q$ , which shows a clear cloud regime dependence, i.e., a Sc-to-Cu increase. The constant  $E_q = 3.2$  used in the current CAM5.3 model overestimates and estimates the observed  $E_q$  in the Sc and Cu regions, respectively.
  3. The  $E_q$  based on the Lognormal PDF assumption performs significantly better than that based on the Gamma PDF assumption. A simple parameterization scheme is provided to relate  $E_q$  to the grid-mean liquid cloud fraction, which can be readily used in GCMs.
  4. For the first time, the enhancement factor  $E_N$  due to the subgrid variation of CDNC is derived from satellite observation, and the results reveal several regions downwind of biomass burning aerosols (e.g., Gulf of Guinea, East Coast of South Africa), air pollution (i.e., Eastern China Sea), and active volcanos (e.g., Kilauea Hawaii and Ambae Vanuatu). The largest  $E_N$  is usually found where CDNC is large and liquid cloud fraction is small and decreases with decreasing CDNC and increasing cloud fraction.
  5. MODIS observations suggest that the subgrid LWP and CDNC are mostly positively correlated. As a result, the combined enhancement factor is significantly smaller than the simple product of  $E_q \cdot E_N$  (i.e., assuming no correlation). The combined enhancement factor derived assuming LWP and CDNC to follow the bi-variate lognormal distribution agree with the observation-based results reasonably well.
- As noted in the previous sections, this study has several important limitations, most of which are a result of using the level-3 MODIS observations. The fixed  $1^\circ \times 1^\circ$  spatial resolution of MODIS level-3 product makes it impossible for us to investigate the scale-dependence of subgrid cloud variation. Similar to previous studies, we have to make several assumptions when estimating the CDNC from level-3 MODIS product. Furthermore, the retrieval uncertainties associated with the optically thin clouds in MODIS product pose a challenging obstacle for the quantification of subgrid cloud property variations and the corresponding enhancement factors. These limitations have to be addressed using additional independent observations from, for

**Deleted:** slightly

**Deleted:** ¶

**Deleted:** ), where the  $E_N$  is comparable, or even larger than  $E_q$ , even after the optically thin clouds are screened out...

**Moved (insertion) [30]**

**Deleted:** In future studies, we will further investigate the implications of these findings from observations for warm rain simulations in GCMs. For example, the parameterization scheme of  $E_q(f_{liq})$  in Eq. (27) can be implemented in the GCMs and compared to the results based on the constant  $E_q$  assumption to understand the potential influence of considering a cloud-regime-dependent  $E_q$  on cloud simulations. Recently, a few novel methods have been developed to provide certain information on the subgrid cloud property variations to the host GCM. Most noticeable examples are the super-parameterization method (a.k.a. multi-scale modeling framework) (Wang et al., 2015) and the higher-order turbulence closure methods (e.g., Cloud Layer Unified By Binormals, CLUBB) (Golaz et al., 2002a; Guo et al., 2015; Larson et al., 2002). Those GCMs coupled with these new schemes, theoretically, would no longer need the enhancement factor. Nevertheless, the subgrid cloud property variations derived in this study provide the observational basis for the evaluation and improvement of these schemes. ¶

As noted in the previous sections, this study has several important limitations, most of which are a result of using the level-3 MODIS observations. The fixed  $1^\circ \times 1^\circ$  spatial resolution of MODIS level-3 product makes it impossible for us to investigate the scale-dependence of subgrid cloud variation. Similar to previous studies, we have to make several assumptions when estimating the CDNC from level-3 MODIS product. Furthermore, the retrieval uncertainties associated with the optically thin clouds in MODIS product pose a challenging obstacle for the quantification of subgrid cloud property variations and the corresponding enhancement factors. These limitations have to be addressed using additional independent observations from, for example, ground based remote sensing product and/or in situ measurement from air-borne field campaigns. Nevertheless, the results from this study provide a valuable roadmap for future studies. ¶

**Acknowledgement:** ¶

Z. Zhang acknowledges the financial support from the Regional and Global Climate Modeling Program (Grant DE-SC0014641) funded by the Office of Biological and Environmental Research in the US DOE Office of Science.

1459 [example, ground based remote sensing product and/or in situ measurement from air-borne field](#)  
1460 [campaigns. Recently, a few novel methods have been developed to provide certain information](#)  
1461 [on the subgrid cloud property variations to the host GCM. Most noticeable examples are the](#)  
1462 [super-parameterization method \(a.k.a. multi-scale modeling framework\) \(Wang et al., 2015\) and](#)  
1463 [the PDF-based higher-order turbulence closure methods \(e.g., Cloud Layer Unified By Binormals,](#)  
1464 [CLUBB \(Golaz et al., 2002a; Guo et al., 2015; Larson et al., 2002\) and Eddy-Diffusivity Mass-Flux](#)  
1465 [\(EDMF\) \(Sušelj et al., 2013\)\). The subgrid cloud property variations derived in this study provide](#)  
1466 [the valuable observational basis for the evaluation and improvement of these schemes.](#)  
1467

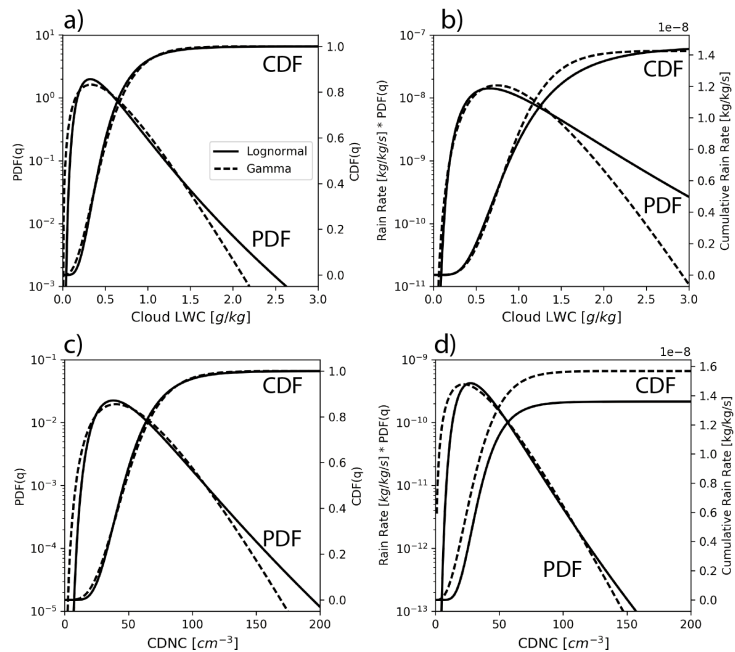
1468  
1469  
1470  
1471  
1472  
1473  
1474  
1475  
1476  
1477  
1478  
1479  
1480  
1481  
1482  
1483  
1484  
1485  
1486

**Acknowledgement:**

Z. Zhang acknowledges the financial support from the Regional and Global Climate Modeling Program (Grant DE-SC0014641) funded by the Office of Biological and Environmental Research in the US DOE Office of Science. This work is also supported by the grant CyberTraining: DSE: Cross-Training of Researchers in Computing, Applied Mathematics and Atmospheric Sciences using Advanced Cyberinfrastructure Resources from the National Science Foundation (grant no. OAC-1730250). P.-L. Ma was support by the U.S. DOE, Office of Science, Office of Biological and Environmental Research, Regional and Global Model Analysis program. The Pacific Northwest National Laboratory is operated for the DOE by Battelle Memorial Institute under contract DE-AC05-76RL01830. V. Larson is grateful for financial support from Climate Model Development and Validation grant DE-SC0016287, which is funded by the Office of Biological and Environmental Research in the US DOE Office of Science. M. Wang was supported by the Minister of Science and Technology of China (2017YFA0604001). The computations in this study were performed at the UMBC High Performance Computing Facility (HPCF). The facility is supported by the U.S. National Science Foundation through the MRI program (Grants CNS-0821258 and CNS-1228778) and the SCREMS program (Grant DMS-0821311), with substantial support from UMBC.

Formatted: Justified

1487  
1488 Figures:



1489  
1490 Figure 1 a) The probability density function (PDF) and cumulative distribution function (CDF) of  
1491 cloud LWC ( $q_c$ ) that follow the Gamma (dashed) and Lognormal (solid) distribution. For the both  
1492 distributions,  $\langle q_c \rangle = 0.5 \text{ g/kg}$  and  $\nu_q = 3.0$ . b) The PDF and CDF of autoconversion rate  
1493 computed based on the KK2000 scheme in Eq. (15) and the PDF of  $q_c$ . In the computation, the  $N_c$   
1494 is kept at a constant of  $50 \text{ cm}^{-3}$ . c) The PDF and CDF of  $N_c$  that follow the Gamma (dashed) and  
1495 Lognormal (solid) distribution. For the both distributions,  $\langle N_c \rangle = 50 \text{ cm}^{-3}$  and  $\nu_N = 5.0$ . d) the  
1496 PDF and CDF of the autoconversion rate computed based on the KK2000 scheme in Eq. (15) and  
1497 the PDF of  $N_c$ . The  $q_c$  is kept at  $0.5 \text{ g/kg}$  in the computation.

1498

Commented [VL29]: Which lines correspond to PDF and which correspond to the CDF? Can this be labeled more precisely?

Formatted: Justified

Deleted:  $\langle LWC \rangle =$

Deleted:  $\nu =$

Deleted: rain

Deleted: (12)

Deleted: LWC.

Deleted: CDNC

Commented [VL30]: Panels c) and d) are not described.

Commented [VL31]: Which lines correspond to PDF and which correspond to the CDF? Can this be labeled more precisely?

Deleted: CDNC

Deleted:  $\nu =$

Deleted: rain

Deleted: (12)

Deleted: CDNC.

Deleted: LWC



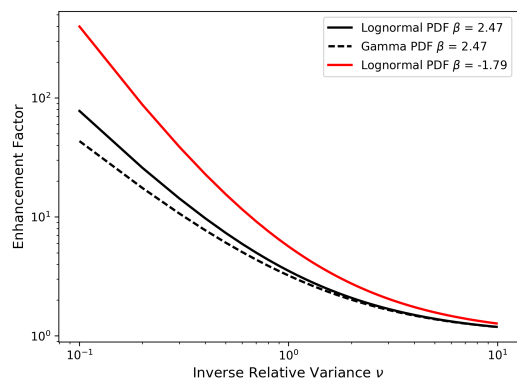


Figure 2 Enhancement factors based on Lognormal  $E(P_L, \beta)$  and Gamma  $E(P_G, \beta)$  subgrid PDF for different  $\beta$  as a function of the inverse relative variance  $v$ .

1515

1516  
1517  
1518  
1519

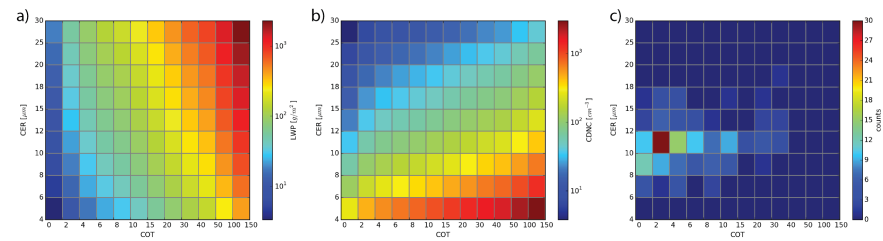
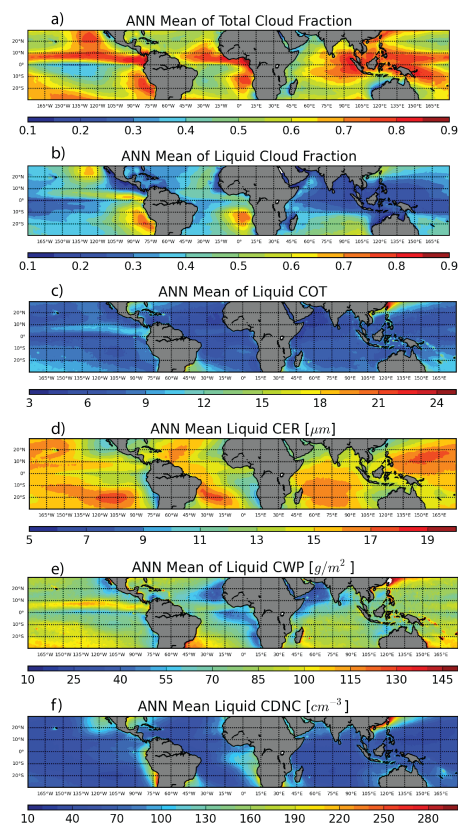


Figure 3 The (a) LWP and (b) CDNC as a function of COT and CER. (c) An exmaple of the COT-CER joint histogram observed by Aqua-MODIS on Jan. 09<sup>th</sup>, 2007 at 1°S and 1°W.

1520  
1521



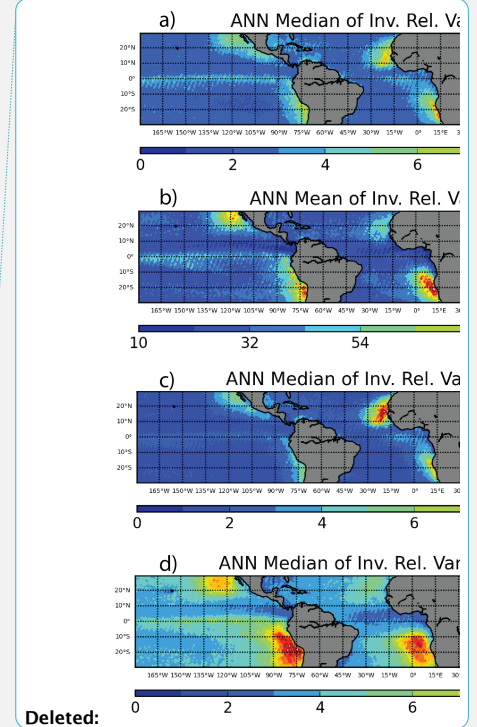
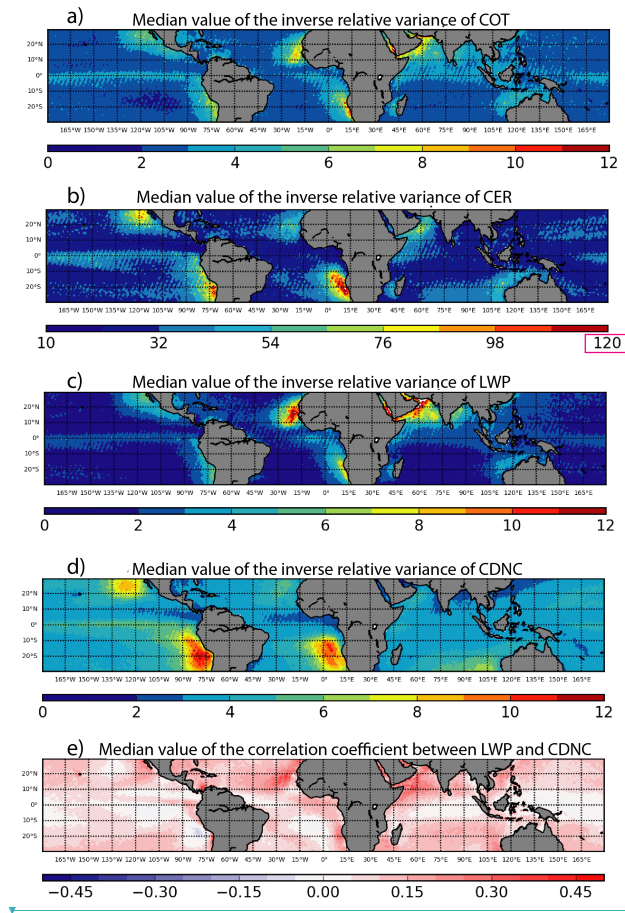
1522

1523 *Figure 4* 10-year (2007~2016) averaged annual mean a) total cloud fraction, b) liquid cloud  
1524 fraction, c) cloud optical thickness, d) cloud effective radius retrieved from the 3.7  $\mu\text{m}$  band, e)  
1525 cloud wather path and f) cloud droplet concentration retrievals from Aqua-MODIS over the  
1526 tropical (30° S-30° N) oceans. All quantaties are “in-cloud” mean that are averaged over the  
1527 cloudy-part of the grid only.

1528

Commented [V32]: This is within-cloud, not grid-box-averaged, right?

Commented [zz33R32]: correct



Deleted:

Deleted: 10-year (2007~2016) averaged annual mean

Deleted: of

Deleted: .

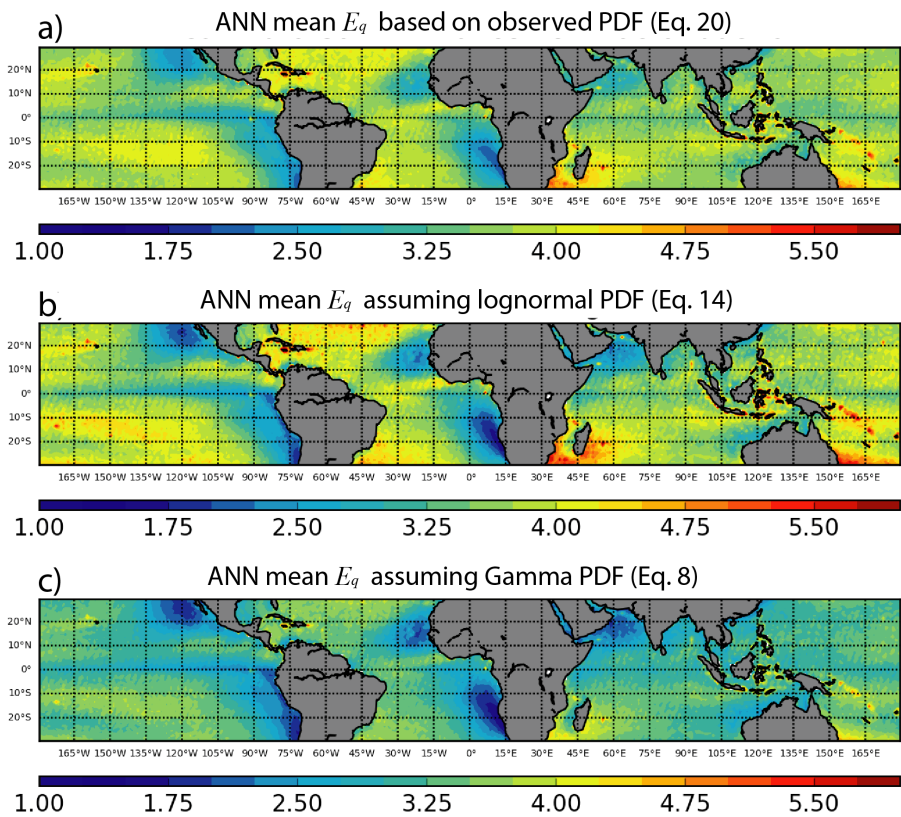
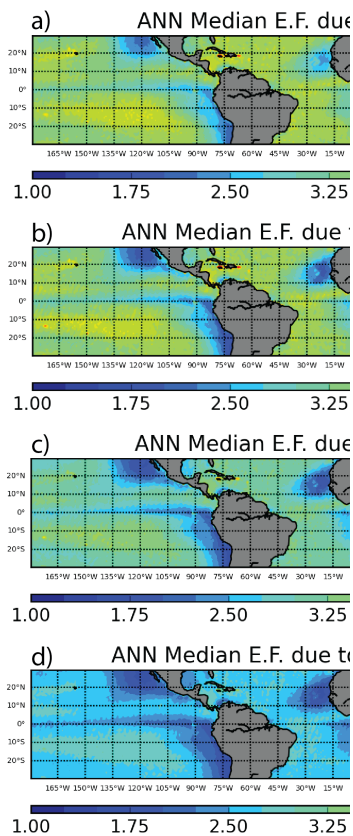
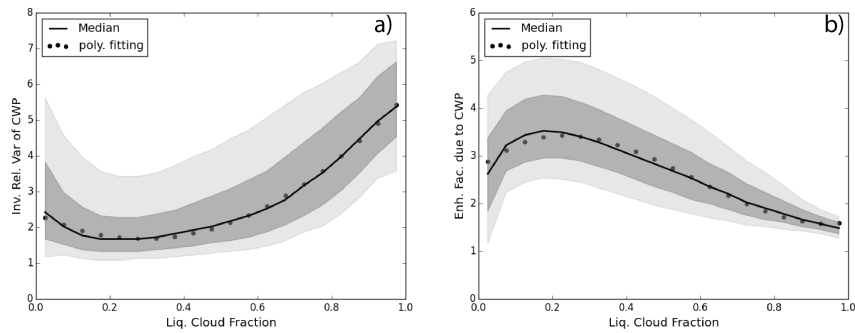


Figure 6 The annual mean factor for the KK2000 scheme due to subgrid variation of LWP computed a) directly from observation, i.e.,  $E_q$  in Eq.(20), b) from relative variance assuming Lognormal PDF of LWP, i.e.,  $E_q$  in Eq.(14) and c) from relative variance assuming the Gamma PDF of LWP, i.e.,  $E_q$  in Eq.(8).



Deleted:  
Deleted: median enhancement  
Commented [V34]: Why is  $E_q$  larger in the shallow cumulus regions than what Lebsock et al. find in their Fig. 7?  
Deleted: . (17),  
Commented [V35]: What is panel d)? There is no description in the caption.  
Deleted: .



*Figure 7* a) The inverse relative variance  $\nu$  and b) autoconversion enhancement factor due to LWP subgrid variability assuming Log-normal PDF as a function of grid-mean liquid cloud fraction, where the solid line, dark shaded area, and light shaded area correspond to the median value, 25%~75% percentiles, and 10~90% percentiles, respectively. The dotted lines correspond to simple 3-rd order polynomial fitting.

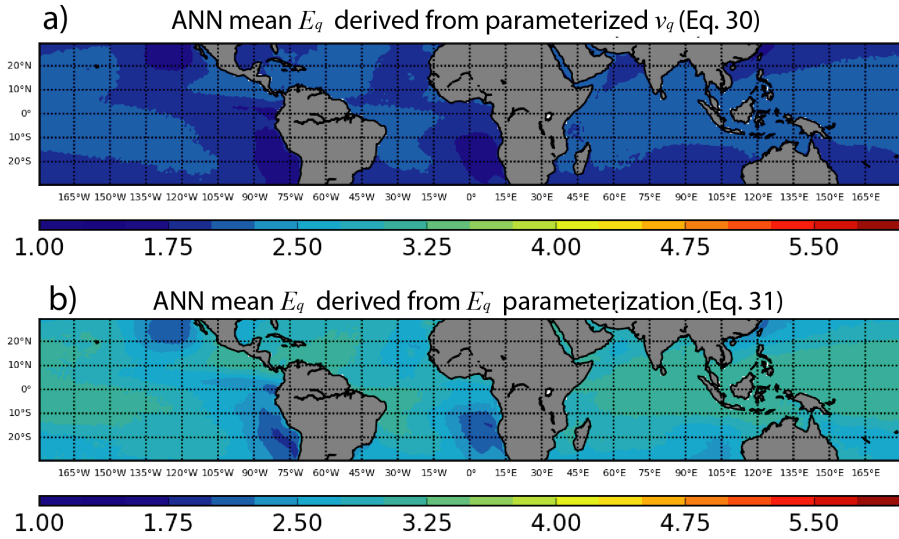
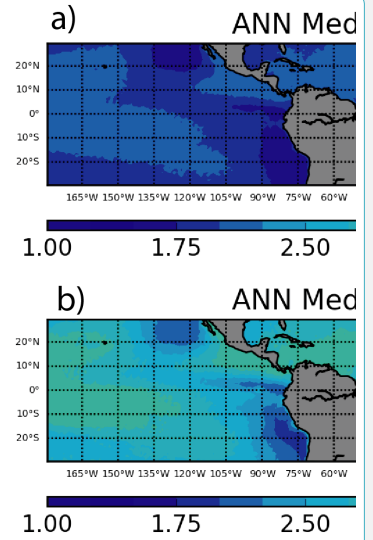


Figure 8 Annual mean value of the enhancement factor  $E_N$  computed based on the a)  $\nu(f_{liq}) = 2.38 - 4.95f_{liq} + 8.74f_{liq}^2 - 0.49f_{liq}^3$  parameterization scheme in Eq. (30) and b)  $E_q(f_{liq}) = 2.72 + 7.33f_{liq} - 19.17f_{liq}^2 + 10.69f_{liq}^3$  parameterization scheme in Eq. (31).



Deleted:

Deleted: Median

Deleted: ( $f_{liq}$ )

Formatted: Font: Not Italic



1567  
1568  
1569

1570  
1571  
1572  
1573

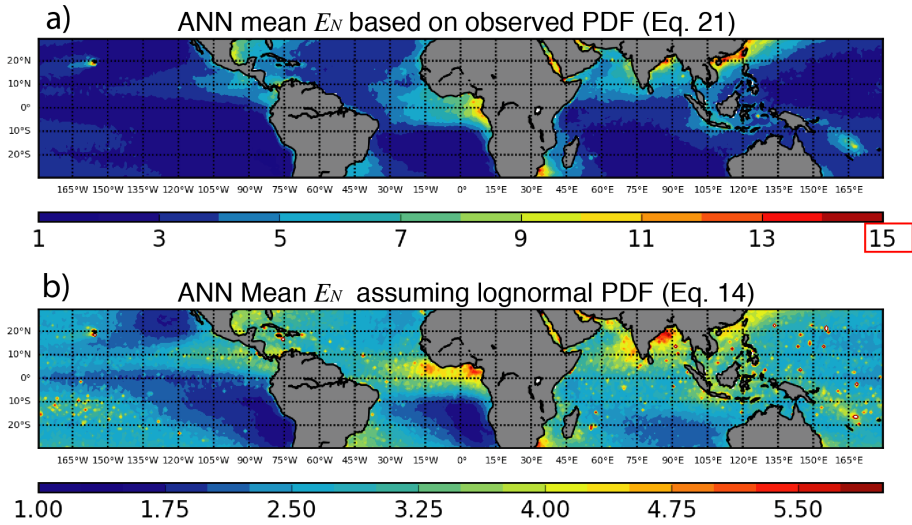
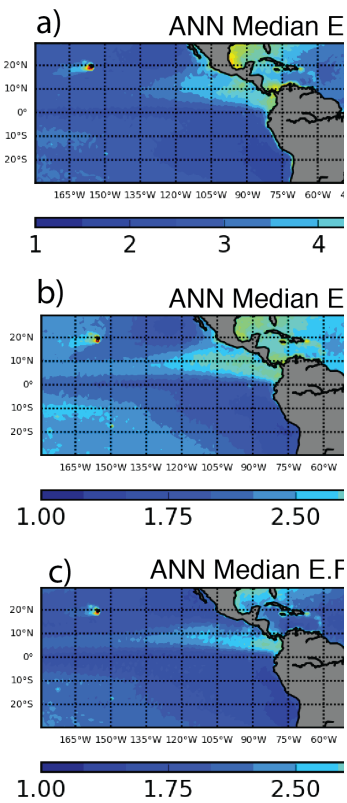


Figure 9 Annual mean value of the enhancement factor  $E_N$  derived from a) observation based on Eq. (21) and b) from Eq. (14) assuming Lognormal subgrid CDNC distribution.



Deleted:

Deleted: Median

Deleted: c) same as a) except that thin clouds with COT < 4 have been screened out from the analysis.

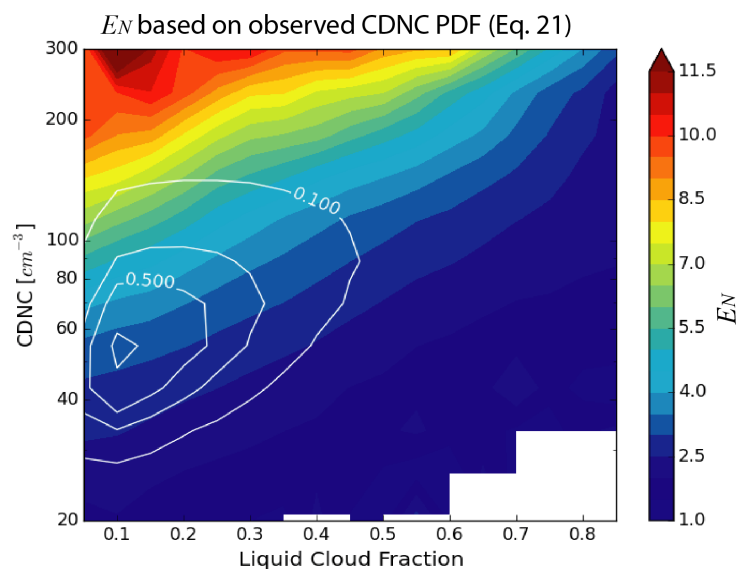
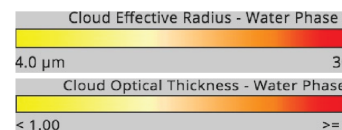
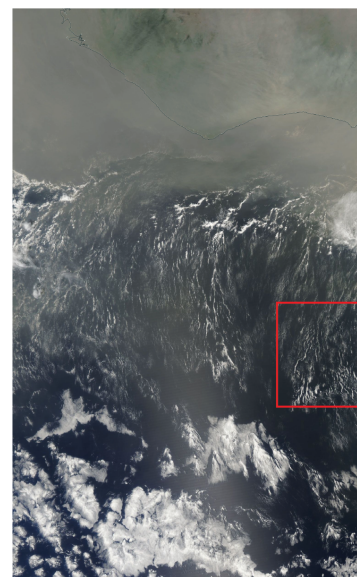


Figure 10 Dependence of  $E_N$  on  $f_{liq}$  and  $N_d$ . The color map corresponds to the mean value of  $E_N$  for a given  $N_d$  and  $f_{liq}$  bin. The white contour lines correspond to the relative sampling frequency of  $N_d$  and  $f_{liq}$  bins (i.e., the most frequently observed combination is  $N_d \sim 50 \text{ cm}^{-3}$  and  $f_{liq} \sim 0.1$ ).



Deleted:

Deleted: An example

Deleted: the large  $E_N$  in the Gulf of Guinea observed by

Deleted: Jan.09<sup>th</sup>, 2007.

Deleted: large image on the left shows the true

Deleted: image of the region.

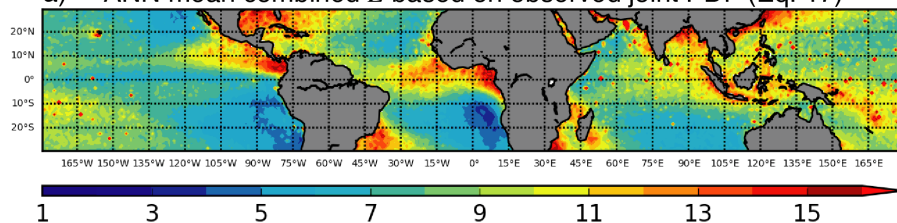
Deleted: three smaller images on the right are, from top to bottom, the zoom-in RGB image, CER and COT retrievals of the subregion in red box.

Formatted: Font: Italic

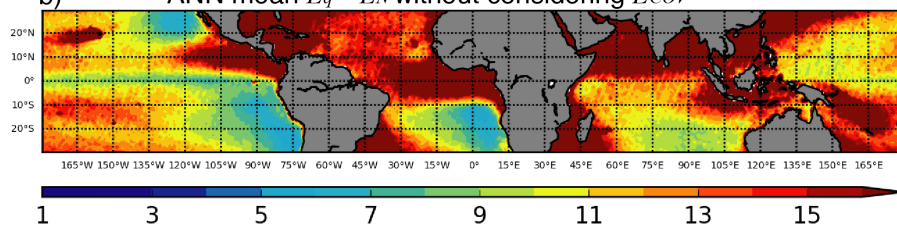
Deleted: .....Page Break.....

... [22]

a) ANN mean combined  $E$  based on observed joint PDF (Eq. 17)



b) ANN mean  $E_q \cdot E_N$  without considering  $E_{cov}$



c) ANN mean combined  $E$  assuming bi-variate lognormal PDF (Eq.23)

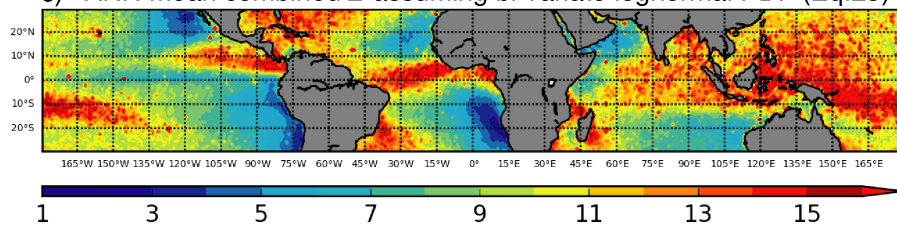


Figure 11 The combined enhancement factor derived a) based on Eq. (17) from the observed joint PDF of LWP and CDNC, b) assuming that subgrid variations of LWP and CDNC are uncorrelated, i.e.,  $E_q \cdot E_N$  only and c) based on Eq. (23) assuming that the subgrid LWP and CDNC following the bi-variate lognormal distribution.

Deleted: a) the

Deleted: (15),

Deleted: the combined enhancement factor based on the assumption...

Deleted: ( $COT > 4$ ). Optical thin clouds ( $COT < 4$ ) are screened out in the computation of  $E_N$  to reduce the impact of retrieval artifacts

Formatted: Font: Italic

1616  
1617

1618 **Reference:**

1619 Ackerman, S., Strabala, K., Menzel, W., Frey, R., Moeller, C. and Gumley, L.: Discriminating clear  
1620 sky from clouds with MODIS, *Journal of Geophysical Research*, 103(D24), 32,141–32,157, 1998.

1621 [Ahlgrimm, M. and Forbes, R. M.: Regime dependence of cloud condensate variability observed  
1622 at the Atmospheric Radiation Measurement Sites, \*Quarterly Journal of the Royal  
1623 Meteorological Society\*, 142\(697\), 1605–1617, doi:10.1002/qj.2783, 2016.](#)

1624 Barker, H. W.: A Parameterization for Computing Grid-Averaged Solar Fluxes for  
1625 Inhomogeneous Marine Boundary Layer Clouds. Part I: Methodology and Homogeneous Biases,  
1626 *J. Atmos. Sci.*, 53(16), 2289–2303, doi:10.1175/1520-0469(1996)053<2289:APFCGA>2.0.CO;2,  
1627 1996.

1628 Barker, H. W., Wiellicki, B. A. and Parker, L.: A Parameterization for Computing Grid-Averaged  
1629 Solar Fluxes for Inhomogeneous Marine Boundary Layer Clouds. Part II: Validation Using  
1630 Satellite Data, [http://dx.doi.org/10.1175/1520-0469\(1996\)053<2304:APFCGA>2.0.CO;2](http://dx.doi.org/10.1175/1520-0469(1996)053<2304:APFCGA>2.0.CO;2), 53(16),  
1631 2304–2316 [online] Available from: <http://journals.ametsoc.org/doi/pdf/10.1175/1520-0469%281996%29053%3C2304%3AAPFCGA%3E2.0.CO%3B2>, 1996.

1633 Bennartz, R.: Global assessment of marine boundary layer cloud droplet number concentration  
1634 from satellite, *Journal of Geophysical Research-Atmospheres*, 2007.

1635 Bennartz, R. and Rausch, J.: Global and regional estimates of warm cloud droplet number  
1636 concentration based on 13 years of AQUA-MODIS observations, *Atmospheric Chemistry and  
1637 Physics*, 1–32, doi:10.5194/acp-2016-1130, 2017.

1638 Bogenschutz, P. A., Gettelman, A., [Hannay, C., Larson, V. E., Neale, R. B., Craig, C. and Chen, C.-  
1639 C.: The Path to CAM6: Coupled Simulations with CAM5.4 and CAM5.5, \*Geosci. Model Dev.\*, 1–  
1640 38, doi:10.5194/gmd-2017-129, 2017.](#)

1641 [Bogenschutz, P. A., Gettelman, A., MORRISON, H., Larson, V. E., Craig, C. and Schanen, D. P.:](#)  
1642 Higher-Order Turbulence Closure and Its Impact on Climate Simulations in the Community  
1643 Atmosphere Model, *J. Climate*, 26(23), 9655–9676, doi:10.1175/JCLI-D-13-00075.1, 2013.

1644 Bony, S. and Dufresne, J.-L.: Marine boundary layer clouds at the heart of tropical cloud  
1645 feedback uncertainties in climate models, *Geophysical Research Letters*, 32(20), L20806,  
1646 doi:10.1029/2005GL023851, 2005.

1647 Boutle, I. A., Abel, S. J., Hill, P. G. and Morcrette, C. J.: Spatial variability of liquid cloud and rain:  
1648 observations and microphysical effects, *Quarterly Journal of the Royal Meteorological Society*,  
1649 140(679), 583–594, doi:10.1002/qj.2140, 2014.

Formatted: Font color: Auto

Deleted: Andreae, M. O. and Merlet, P.: Emission of trace  
gases and aerosols from biomass burning, *Global  
Biogeochemical Cycles*, 15(4), 955–966,  
doi:10.1029/2000GB001382, 2001. ¶

Formatted: Font color: Auto

Formatted: Font color: Auto

Deleted: . and Abel, S. J.: Microphysical controls on the  
stratocumulus topped boundary-layer structure during  
VOCALS-REx, *Atmospheric Chemistry and Physics*, 12(6),  
2849–2863, doi:10.5194/acp-12-2849-2012, 2012. ¶  
Boutle, I. A

Formatted: Font color: Auto

1659 Cahalan, R. F., Ridgway, W., Wiscombe, W. J., Bell, T. L. and Snider, J. B.: The Albedo of Fractal  
1660 Stratocumulus Clouds, *J. Atmos. Sci.*, 51(16), 2434–2455, doi:10.1175/1520-  
1661 0469(1994)051<2434:TAOFSC>2.0.CO;2, 1994.

1662 Cho, H. M., Zhang, Z., Meyer, K., Lebsock, M., Platnick, S., Ackerman, A. S., Di Girolamo, L., C  
1663 Labonnote, L., Cornet, C., Riedi, J. and Holz, R. E.: Frequency and causes of failed MODIS cloud  
1664 property retrievals for liquid phase clouds over global oceans, *Journal of Geophysical Research-*  
1665 *Atmospheres*, 120(9), 2015JD023161–n/a, doi:10.1002/2015JD023161, 2015.

1666 Considine, G., Curry, J. A. and Wielicki, B.: Modeling cloud fraction and horizontal variability in  
1667 marine boundary layer clouds, *J. Geophys. Res.*, 102(D12), 13517–13525, 1997.

1668 [Eyring, V., Bony, S., Meehl, G. A., Senior, C. A., Stevens, B., Stouffer, R. J. and Taylor, K. E.:  
1669 \[Overview of the Coupled Model Intercomparison Project Phase 6 \\(CMIP6\\) experimental design  
1670 and organization\]\(#\), \*Geosci. Model Dev.\*, 9\(5\), 1937–1958, doi:10.5194/gmd-9-1937-2016, 2016.](#)

1671 Golaz, J.-C., Larson, V. E. and Cotton, W. R.: A PDF-Based Model for Boundary Layer Clouds. Part  
1672 I: Method and Model Description, *JAS*, 59(24), 3540–3551, doi:10.1175/1520-  
1673 0469(2002)059<3540:APBMFB>2.0.CO;2, 2002a.

1674 Golaz, J.-C., Larson, V. E. and Cotton, W. R.: A PDF-Based Model for Boundary Layer Clouds. Part  
1675 II: Model Results, [http://dx.doi.org/10.1175/1520-0469\(2002\)059<3552:APBMFB>2.0.CO;2](http://dx.doi.org/10.1175/1520-0469(2002)059<3552:APBMFB>2.0.CO;2),  
1676 59(24), 3552–3571, doi:10.1175/1520-0469(2002)059<3552:APBMFB>2.0.CO;2, 2002b.

1677 Griffin, B. M. and Larson, V. E.: Analytic upscaling of a local microphysics scheme. Part II:  
1678 Simulations, *Quarterly Journal of the Royal Meteorological Society*, 139(670), 58–69,  
1679 doi:10.1002/qj.1966, 2013.

1680 Grosvenor, D. P. and Wood, R.: The effect of solar zenith angle on MODIS cloud optical and  
1681 microphysical retrievals within marine liquid water clouds, *Atmospheric Chemistry and Physics*,  
1682 14(14), 7291–7321, doi:10.5194/acpd-14-303-2014, 2014.

1683 Grosvenor, D. P., Sourdeval, O., Zuidema, P., Ackerman, A., Alexandrov, M. D., Bennartz, R.,  
1684 Cairns, B., Chiu, C., Christensen, M., Diamond, M., Feingold, G., Fridlind, A., Hunerbein, A., Knist,  
1685 C., Kollias, P., Marshak, A., McCoy, D., Merk, D., Painemal, D., Rausch, J., Rosenfeld, D.,  
1686 Russchenberg, H., Seifert, P., Sinclair, K., Stier, P., vanDiedenhoven, B., Wendisch, M., Werner,  
1687 F., Wood, R., Zhang, Z. and Quaas, J.: **Remote sensing of droplet number concentration in**  
1688 **warm clouds: A review of the current state of knowledge and perspectives**, *Reviews of*  
1689 *Geophysics*, (in review), 2018.

1690 Gultepe, I. and Isaac, G. A.: Aircraft observations of cloud droplet number concentration:  
1691 Implications for climate studies, *Quarterly Journal of the Royal Meteorological Society*,  
1692 130(602), 2377–2390, doi:10.1256/qj.03.120, 2004.

Formatted: Font color: Auto

1693 Guo, H., Golaz, J. C., Donner, L. J., [Larson, V. E., Schanen, D. P. and Griffin, B. M.: Multi-variate](#)  
1694 [probability density functions with dynamics for cloud droplet activation in large-scale models:](#)  
1695 [single column tests, Geosci. Model Dev., 3\(2\), 475–486, doi:10.5194/gmd-3-475-2010, 2010.](#)

1696 [Guo, H., Golaz, J. C., Donner, L. J., Wyman, B., Zhao, M. and Ginoux, P.: CLUBB as a unified cloud](#)  
1697 [parameterization: Opportunities and challenges, Geophysical Research Letters, 42\(11\), 4540–](#)  
1698 [4547, doi:10.1002/2015GL063672, 2015.](#)

1699 Guo, Z., Wang, M., Qian, Y., Larson, V. E., Ghan, S., Ovchinnikov, M., Bogenschutz, P. A., Zhao,  
1700 C., Lin, G. and Zhou, T.: A sensitivity analysis of cloud properties to CLUBB parameters in the  
1701 single-column Community Atmosphere Model (SCAM5), J. Adv. Model. Earth Syst., 6(3), 829–  
1702 858, doi:10.1002/2014MS000315, 2014.

1703 Hill, P. G., Morcrette, C. J. and Boutle, I. A.: A regime-dependent parametrization of subgrid-  
1704 scale cloud water content variability, Quarterly Journal of the Royal Meteorological Society,  
1705 141(691), 1975–1986, doi:10.1002/qj.2506, 2015.

1706 Kawai, H. and Teixeira, J.: Probability Density Functions of Liquid Water Path and Cloud Amount  
1707 of Marine Boundary Layer Clouds: Geographical and Seasonal Variations and Controlling  
1708 Meteorological Factors, <http://dx.doi.org/10.1175/2009JCLI3070.1>, 23(8), 2079–2092,  
1709 doi:10.1175/2009JCLI3070.1, 2010.

1710 Khairoutdinov, M. and Kogan, Y.: A New Cloud Physics Parameterization in a Large-Eddy  
1711 Simulation Model of Marine Stratocumulus, Mon. Wea. Rev, 128(1), 229–243 [online] Available  
1712 from: [http://journals.ametsoc.org/doi/abs/10.1175/1520-](http://journals.ametsoc.org/doi/abs/10.1175/1520-0493(2000)128%3C0229%3AANCPPI%3E2.0.CO%3B2)  
1713 [0493\(2000\)128%3C0229%3AANCPPI%3E2.0.CO%3B2](http://journals.ametsoc.org/doi/abs/10.1175/1520-0493(2000)128%3C0229%3AANCPPI%3E2.0.CO%3B2), 2000.

1714 Klein, S. and Hartmann, D.: The seasonal cycle of low stratiform clouds, Journal of Climate, 6(8),  
1715 1587–1606, 1993.

1716 Kubar, T. L., Stephens, G. L., Lebsock, M., Larson, V. E. and Bogenschutz, P. A.: Regional  
1717 Assessments of Low Clouds against Large-Scale Stability in CAM5 and CAM-CLUBB Using MODIS  
1718 and ERA-Interim Reanalysis Data, J. Climate, 28(4), 1685–1706, doi:10.1175/JCLI-D-14-00184.1,  
1719 2014.

1720 Larson, V. E. and Griffin, B. M.: Analytic upscaling of a local microphysics scheme. Part I:  
1721 Derivation, Quarterly Journal of the Royal Meteorological Society, 139(670), 46–57,  
1722 doi:10.1002/qj.1967, 2013.

1723 Larson, V. E., Golaz, J.-C. and Cotton, W. R.: Small-Scale and Mesoscale Variability in Cloudy  
1724 Boundary Layers: Joint Probability Density Functions, J. Atmos. Sci., 59(24), 3519–3539,  
1725 doi:10.1175/1520-0469(2002)059<3519:SSAMVI>2.0.CO;2, 2002.

1726 Larson, V. E., Wood, R., Field, P. R., Golaz, J.-C., Vonder Haar, T. H. and Cotton, W. R.: Systematic  
1727 Biases in the Microphysics and Thermodynamics of Numerical Models That Ignore Subgrid-Scale

Formatted: Font color: Auto

1728 Variability, J. Atmos. Sci., 58(9), 1117–1128, doi:10.1175/1520-  
 1729 0469(2001)058<1117:SBITMA>2.0.CO;2, 2001.

1730 Lebsock, M. D., L'Ecuyer, T. S. and Stephens, G. L.: [Detecting the Ratio of Rain and Cloud Water](#)  
 1731 [in Low-Latitude Shallow Marine Clouds](#), *Journal of Applied Meteorology and Climatology*, 50(2),  
 1732 [419–432](#), doi:10.1175/2010JAMC2494.1, 2011.

1733 [Lebsock, M.](#), MORRISON, H. and Gettelman, A.: Microphysical implications of cloud-  
 1734 precipitation covariance derived from satellite remote sensing, *Journal of Geophysical*  
 1735 *Research-Atmospheres*, 118(12), 6521–6533, doi:10.1002/jgrd.50347, 2013.

1736 Lee, S., Kahn, B. H. and Teixeira, J.: Characterization of cloud liquid water content distributions  
 1737 from CloudSat, *J. Geophys. Res.*, 115(D20), D00A23, doi:10.1029/2009JD013272, 2010.

1738 McCoy, D. T., Bender, F. A. M., Grosvenor, D. P., Mohrmann, J. K., Hartmann, D. L., Wood, R.  
 1739 and Field, P. R.: Predicting decadal trends in cloud droplet number concentration using  
 1740 reanalysis and satellite data, *Atmospheric Chemistry and Physics*, 1–21, 2017a.

1741 McCoy, D. T., Bender, F. A. M., Mohrmann, J. K. C., Hartmann, D. L., Wood, R. and Grosvenor, D.  
 1742 P.: The global aerosol-cloud first indirect effect estimated using MODIS, MERRA, and AeroCom,  
 1743 *Journal of Geophysical Research-Atmospheres*, 122(3), 1779–1796, doi:10.1002/2016JD026141,  
 1744 2017b.

1745 Menzel, P., Frey, R., Baum, B. and Zhang, H.: Cloud Top Properties and Cloud Phase Algorithm  
 1746 Theoretical Basis Document. 2006.

1747 Menzel, W., Smith, W. and Stewart, T.: Improved Cloud Motion Wind Vector and Altitude  
 1748 Assignment Using VAS, *Journal of Applied Meteorology*, 22(3), 377–384, 1983.

1749 Morales, R. and Nenes, A.: Characteristic updrafts for computing distribution-averaged cloud  
 1750 droplet number and stratocumulus cloud properties, *J. Geophys. Res.*, 115(D18), 1227, 2010.

1751 Morrison, H. and Gettelman, A.: A new two-moment bulk stratiform cloud microphysics scheme  
 1752 in the Community Atmosphere Model, version 3 (CAM3). Part I: Description and numerical  
 1753 tests, *Journal of Climate*, 2008.

1754 Nakajima, T. and King, M. D.: Determination of the Optical Thickness and Effective Particle  
 1755 Radius of Clouds from Reflected Solar Radiation Measurements. Part I: Theory, *J. Atmos. Sci.*,  
 1756 47(15), 1878–1893, doi:10.1175/1520-0469(1990)047<1878:DOTOTA>2.0.CO;2, 1990.

1757 Nam, C., Bony, S., Dufresne, J. L. and Chepfer, H.: The “too few, too bright” tropical low-cloud  
 1758 problem in CMIP5 models, *Geophysical Research ...*, doi:10.1029/2012GL053421, 2012.

1759 Oreopoulos, L. and Barker, H. W.: Accounting for subgrid-scale cloud variability in a multi-layer  
 1760 1d solar radiative transfer algorithm, *Quarterly Journal of the Royal Meteorological Society*,  
 1761 125(553), 301–330, doi:10.1002/qj.49712555316, 1999.

Formatted: Font color: Auto



1762 Oreopoulos, L. and Cahalan, R. F.: Cloud Inhomogeneity from MODIS, *Journal of Climate*,  
1763 18(23), 5110–5124, doi:10.1175/JCLI3591.1, 2005.

1764 Oreopoulos, L. and Davies, R.: Plane Parallel Albedo Biases from Satellite Observations. Part I:  
1765 Dependence on Resolution and Other Factors, *Journal of Climate*, 11(5), 919–932, 1998a.

1766 Oreopoulos, L. and Davies, R.: Plane Parallel Albedo Biases from Satellite Observations. Part II:  
1767 Parameterizations for Bias Removal, *J. Climate*, 11(5), 933–944, 1998b.

1768 Pincus, R. and Klein, S. A.: Unresolved spatial variability and microphysical process rates in  
1769 large-scale models, *J. Geophys. Res.*, 105(D22), 27059–27065, doi:10.1029/2000JD900504,  
1770 2000.

1771 Platnick, S., King, M. D., Ackerman, S. A., Menzel, W. P., Baum, B. A., Riédi, J. C. and Frey, R. A.:  
1772 The MODIS cloud products: algorithms and examples from Terra, *IEEE TRANSACTIONS ON*  
1773 *GEOSCIENCE AND REMOTE SENSING*, 41(2), 459–473, doi:10.1109/TGRS.2002.808301, 2003.

1774 Platnick, S., Meyer, K. G., King, M. D., Wind, G., Amarasinghe, N., Marchant, B., Arnold, G. T.,  
1775 Zhang, Z., Hubanks, P. A., Holz, R. E., Yang, P., Ridgway, W. L. and Riedi, J.: The MODIS Cloud  
1776 Optical and Microphysical Products: Collection 6 Updates and Examples From Terra and Aqua,  
1777 *IEEE TRANSACTIONS ON GEOSCIENCE AND REMOTE SENSING*, 55(1), 502–525,  
1778 doi:10.1109/TGRS.2016.2610522, 2017.

1779 Pruppacher, H. R. and Klett, J. D.: *Microphysics of Clouds and Precipitation: With an*  
1780 *Introduction to Cloud Chemistry and Cloud Electricity*, 954 pp. 1997.

1781 [Randall, D., Khairoutdinov, M., Arakawa, A. and Grabowski, W.: Breaking the Cloud](#)  
1782 [Parameterization Deadlock, \*Bulletin of the American Meteorological Society\*, 84\(11\), 1547–](#)  
1783 [1564, doi:10.1175/BAMS-84-11-1547, 2003.](#)

1784 Seethala, C. and Horváth, Á.: Global assessment of AMSR-E and MODIS cloud liquid water path  
1785 retrievals in warm oceanic clouds, *J Geophys Res*, 115(D13), D13202, 2010.

1786 Soden, B. and Held, I.: An assessment of climate feedbacks in coupled ocean–atmosphere  
1787 models, *Journal of Climate*, 2006.

1788 Song, H., Song, H., Zhang, Z., Ma, P.-L., Ghan, S. J. and Wang, M.: An Evaluation of Marine  
1789 Boundary Layer Cloud Property Simulations in the Community Atmosphere Model Using  
1790 Satellite Observations: Conventional Subgrid Parameterization versus CLUBB, *Journal of*  
1791 *Climate*, 31(6), 2299–2320, doi:10.1175/JCLI-D-17-0277.1, [2018a](#).

1792 Song, H., Zhang, Z., Ma, P.-L., Ghan, S. J. and Wang, M.: An Evaluation of Marine Boundary Layer  
1793 Cloud Property Simulations in [the](#) Community Atmosphere Model Using Satellite Observations:  
1794 Conventional [Subgrid](#) Parameterization [versus](#) CLUBB, *Journal of Climate*, [31\(6\), 2299–2320](#),  
1795 doi:10.1175/JCLI-D-17-0277.1, [2018b](#).

**Deleted:** ",rightsLink":"http://s100.copyright.com/AppDis  
patchServlet?publisherName=ieee&publication=0196-  
2892&title=The+MODIS+Cloud+Optical+and+Microphysical+  
Products%3A+Collection+6+Updates+and+Examples+From+  
Terra+and+Aqua&isbn=&publicationDate=Jan.+2017&autho  
r=Steven+Platnick&ContentID=10.1109/TGRS.2016.2610522  
&orderBeanReset=true&startPage=502&endPage=525&vol  
umeNum=55&issueNum=1",displayPublicationTitle":"IEEE

**Formatted:** Font color: Auto

**Deleted:** Quaas, J., Boucher, O., Bellouin, N. and Kinne, S.:  
Satellite-based estimate of the direct and indirect aerosol  
climate forcing, *J. Geophys. Res.*, 113(D5), n/a–n/a,  
doi:10.1029/2007JD008962, 2008.¶

**Formatted:** Font color: Auto

**Deleted:** 2018

**Formatted:** Font color: Auto

**Deleted:** .

**Formatted:** Font color: Auto

**Formatted:** Font color: Auto

**Formatted:** Font color: Auto

**Deleted:** Sub-grid

**Formatted:** Font color: Auto

**Deleted:** vs.

**Formatted:** Font color: Auto

**Deleted:** J.

**Formatted:** Font color: Auto

**Deleted:** JCLI–D–17–0277.1

**Formatted:** Font color: Auto

**Deleted:** 2017

**Formatted:** Font color: Auto

1815 [Sušelj, K., Teixeira, J. and Chung, D.: A Unified Model for Moist Convective Boundary Layers](#)  
1816 [Based on a Stochastic Eddy-Diffusivity/Mass-Flux Parameterization, J. Atmos. Sci., 70\(7\), 1929–](#)  
1817 [1953, doi:10.1175/JAS-D-12-0106.1, 2013.](#)

1818 [Takahashi, H., Lebsock, M., Suzuki, K., Stephens, G. and Wang, M.: An investigation of](#)  
1819 [microphysics and subgrid-scale variability in warm-rain clouds using the A-Train observations](#)  
1820 [and a multiscale modeling framework, Journal of Geophysical Research-Atmospheres, 138\(669\),](#)  
1821 [2151, 2017.](#)

1822 Thayer-Calder, K., Gettelman, A., Craig, C., Goldhaber, S., Bogenschutz, P. A., Chen, C. C.,  
1823 Morrison, H., Höft, J., Raut, E., Griffin, B. M., Weber, J. K., Larson, V. E., Wyant, M. C., Wang, M.,  
1824 Guo, Z. and Ghan, S. J.: A unified parameterization of clouds and turbulence using CLUBB and  
1825 subcolumns in the Community Atmosphere Model, Geosci. Model Dev., 8(12), 3801–3821,  
1826 doi:10.5194/gmd-8-3801-2015, 2015.

1827 Trenberth, K. E., Fasullo, J. T. and Kiehl, J.: Earth's Global Energy Budget, Bull. Amer. Meteor.  
1828 Soc., 90(3), 311–323, doi:10.1175/2008BAMS2634.1, 2009.

1829 Wang, M., Larson, V. E., Ghan, S., Ovchinnikov, M., Schanen, D. P., Xiao, H., Liu, X., Rasch, P. and  
1830 Guo, Z.: A multiscale modeling framework model (superparameterized CAM5) with a higher-  
1831 order turbulence closure: Model description and low-cloud simulations, J. Adv. Model. Earth  
1832 Syst., n/a–n/a, doi:10.1002/2014MS000375, 2015.

1833 Wood, R. and Hartmann, D.: Spatial variability of liquid water path in marine low cloud: The  
1834 importance of mesoscale cellular convection, Journal of Climate, 2006.

1835 Xie, X. and Zhang, M.: Scale-aware parameterization of liquid cloud inhomogeneity and its  
1836 impact on simulated climate in CESM, Journal of Geophysical Research-Atmospheres, 120(16),  
1837 8359–8371, doi:10.1002/2015JD023565, 2015.

1838 Zhang, Z. and Platnick, S.: An assessment of differences between cloud effective particle radius  
1839 retrievals for marine water clouds from three MODIS spectral bands, J Geophys Res, 116(D20),  
1840 D20215, doi:10.1029/2011JD016216, 2011.

1841 Zhang, Z., Ackerman, A. S., Feingold, G., Platnick, S., Pincus, R. and Xue, H.: Effects of cloud  
1842 horizontal inhomogeneity and drizzle on remote sensing of cloud droplet effective radius: Case  
1843 studies based on large-eddy simulations, J Geophys Res, 117(D19), D19208–,  
1844 doi:10.1029/2012JD017655, 2012.

1845 Zhang, Z., Werner, F., Cho, H. M., Wind, G., Platnick, S., Ackerman, A. S., Di Girolamo, L.,  
1846 Marshak, A. and Meyer, K.: A framework based on 2-D Taylor expansion for quantifying the  
1847 impacts of sub-pixel reflectance variance and covariance on cloud optical thickness and  
1848 effective radius retrievals based on the bi-spectral method, Journal of Geophysical Research-  
1849 Atmospheres, 2016JD024837, doi:10.1002/2016JD024837, 2016.

Deleted: Taylor

Deleted: . E., Stouffer, R.

Formatted: Font color: Auto

Deleted: Meehl

Formatted: Font color: Auto

Formatted: Font color: Auto

Deleted: A

Formatted: Font color: Auto

Deleted: Overview

Formatted: Font color: Auto

Deleted: CMIP5 and

Formatted: Font color: Auto

Deleted: Experiment Design, Bulletin

Formatted: Font color: Auto

Deleted: the American Meteorological Society, 93(4),  
485–498, doi:10.1175/BAMS-D-11-00094.1, 2012

Formatted: Font color: Auto

Formatted: Indent: Left: 0", First line: 0"

Page 4: [1] Deleted	Zhibo Zhang	12/3/18 8:08:00 AM
---------------------	-------------	--------------------



Page 4: [2] Deleted	Zhibo Zhang	12/3/18 8:08:00 AM
---------------------	-------------	--------------------



Page 9: [3] Deleted	Zhibo Zhang	12/3/18 8:08:00 AM
---------------------	-------------	--------------------

Page 9: [4] Deleted	Zhibo Zhang	12/3/18 8:08:00 AM
---------------------	-------------	--------------------

Page 10: [5] Deleted	Zhibo Zhang	12/3/18 8:08:00 AM
----------------------	-------------	--------------------



Page 10: [6] Deleted	Zhibo Zhang	12/3/18 8:08:00 AM
----------------------	-------------	--------------------



Page 10: [7] Deleted	Zhibo Zhang	12/3/18 8:08:00 AM
----------------------	-------------	--------------------



Page 10: [8] Deleted	Zhibo Zhang	12/3/18 8:08:00 AM
----------------------	-------------	--------------------



Page 10: [9] Deleted	Zhibo Zhang	12/3/18 8:08:00 AM
----------------------	-------------	--------------------

Page 10: [10] Commented [VL2]	Vincent Larson	5/31/18 9:08:00 AM
-------------------------------	----------------	--------------------

I doubt that this is often true in nature.

Page 12: [11] Deleted	Zhibo Zhang	12/3/18 8:08:00 AM
-----------------------	-------------	--------------------

Page 12: [12] Deleted	Zhibo Zhang	12/3/18 8:08:00 AM
-----------------------	-------------	--------------------



Page 13: [13] Deleted	Zhibo Zhang	12/3/18 8:08:00 AM
-----------------------	-------------	--------------------



Page 19: [14] Deleted	Zhibo Zhang	12/3/18 8:08:00 AM
-----------------------	-------------	--------------------



1.1.

Page 19: [15] Deleted	Zhibo Zhang	12/3/18 8:08:00 AM
-----------------------	-------------	--------------------



Page 19: [16] Deleted	Zhibo Zhang	12/3/18 8:08:00 AM
-----------------------	-------------	--------------------



Page 19: [17] Deleted	Zhibo Zhang	12/3/18 8:08:00 AM
-----------------------	-------------	--------------------



Page 19: [18] Deleted	Zhibo Zhang	12/3/18 8:08:00 AM
-----------------------	-------------	--------------------



Page 22: [19] Deleted	Zhibo Zhang	12/3/18 8:08:00 AM
-----------------------	-------------	--------------------



Page 23: [20] Deleted	Zhibo Zhang	12/3/18 8:08:00 AM
-----------------------	-------------	--------------------



Page 23: [21] Deleted	Zhibo Zhang	12/3/18 8:08:00 AM
-----------------------	-------------	--------------------



Page 37: [22] Deleted	Zhibo Zhang	12/3/18 8:08:00 AM
-----------------------	-------------	--------------------

